Improving Spin Crossover Characteristics in Heteroleptic [Fe^{III}(qsal-5-I)(qsal-5-OMe)]A Complexes

Raúl Díaz-Torres,[a]† Silvia Gómez-Coca,[b] Eliseo Ruiz,[b]
Phimphaka Harding[c]† and David J. Harding[c]†

[a] Thammasat University Research Unit in Multifunctional Crystalline Materials and Applications (TU-MCMA), Faculty of Science and Technology, Thammasat University, Pathum Thani 12121, Thailand.

[b] Departament de Química Inorgànica i Orgànica & IQTC-UB, Universitat de Barcelona, Martí i Franquès, 1-11, 08028 Barcelona, Spain

[c] School of Chemistry, Institute of Science, Suranaree University of Technology, Nakhon Ratchasima, 30000, Thailand

† Previous address: Functional Materials and Nanotechnology Centre of Excellence, Walailak University, Thasala, Nakhon Si Thammarat, 80160, Thailand.

Contents Page No.

Study of [Fe(qsal-I)(qsal-5-OMe)](A) complexes with different anions

Table S1. List of Fe^{III} systems that exhibit significant hysteresis.

Iron(III) Complex	ΔT hysteresis	Ref
$[Fe^{III}(qsal)_2]NCSe\cdot CH_2Cl_2$	76 K	[1]
β-$[Fe(qsal)_2]I_3$	25 K	[2]
$[Fe^{III}(qnal\text{-}OMe)_2]BPh_4\cdot 2MeOH$	110 K	[3]
$[Fe^{III}(qsal\text{-}I)_2]OTf$	8 K	[4]
$[Fe^{III}(H\text{-}5\text{-}Cl\text{-}thsa\text{-}Et)(5\text{-}Cl\text{-}thsa\text{-}Et)]\cdot H_2O$	51 K	[5]
$K[Fe(5\text{-}Br\text{-}thsa)_2]$	52 K	[6]
$[Fe^{III}(qsal\text{-}5\text{-}OMe)(qsal\text{-}I)]OTf$	35 K	This work
$[Fe^{III}(qsal\text{-}I)_2]NTf_2$	34 K	[7]
$[Fe^{III}(naphBzen)_2]I$	30 K*	[8]

*hidden hysteresis

X-ray crystallography further discussion

As noted in the main paper the structures contain disorder of the iodo and methoxy groups. To model this disorder required the iodo and methoxy groups to be split into two parts with occupancies initially refined and then (with the exception of **2**), fixed at values close to those found from the refinement. In all cases DFIX restraints were used for the methoxy groups with the C(aromatic)-O bond set to be 1.38 Å, while the O-CH_3 bond was set to 1.42 Å, with 0.02 Å allowed deviation. In some of the structures the aromatic rings to which the iodo and methoxy groups are attached were also found to be disordered and SADI restraints were applied. More specific details for each structure are given below.

For **1**, the occupancies for the two ligands refine close to 50% at both temperatures and hence the occupancies were fixed at 0.5. The methoxy groups were refined isotropically as anisotropic refinement gave unreasonable ellipsoids. At 300 K the methoxy groups were also constrained with an EADP restraint.

In **2**, the refined occupancies for one of the rings were found to be 0.48 and 0.52 on one of the ligands and 0.34 and 0.66 on the other ligand, indicating an excess of the qsal-5-OMe ligand in the crystal structure. EADP constraints were applied to the methoxy groups and RIGU restraints on the disordered salicylaldimine aromatic carbons. Anisotropic refinement of the NCS^- anion gave strongly elongated ellipsoids indicating possible disorder in the anion. Attempts to model this disorder did not prove effective, possibly due to the proximity of a nearby inversion center. Consequently, we opted to refine the anion isotropically and with full occupancy.

For the BF_4 complex, **3**, the two ligands refine as 0.4 and 0.6 on one of the ligands and 0.6 and 0.4 on the other ligand, meaning that there is a 1:1 ratio overall. The methoxy groups are refined as isotropic with EADP constraints at 150 K. At 300 K only the O3-C33 methoxy group is isotropic, again requiring an EADP constraint. In both structures only the aromatic rings with the O3-C33 methoxy group are disordered with the aromatic carbons refined isotropically. At low temperature the MeOH molecule refines to *ca*. 0.8 occupancy. However, there are a small number of low intensity Q-peaks close to the MeOH that suggest additional solvent molecules may be present, most probably MeOH. Application of a solvent mask was necessary at 300 K and indicates that there are 1.1 MeOH molecules in the structure and this was used in the description of the compound in the main paper.

In **4**, the refined occupancies for one of the rings were found to be 0.48 and 0.52 on one of the ligands and 0.41 and 0.59 on the other ligand, indicating an excess of the qsal-5-I ligand in the crystal structure. As in **2**, EADP constraints were applied to the methoxy groups. At 280 K the methoxy groups are refined isotropically with an EADP constraint applied to the O3-C33 atoms. RIGU restraints were applied to the C12→C15 and C12A→C15A atoms.

In the structure of **6** at 280 K the CH_2Cl_2 molecule was disordered over two positions, in a 40% to 60% ratio. Although the ellipsoids are a little larger than is ideal, application of a solvent mask reveals that 1 equivalent of CH_2Cl_2 is expected and hence the model is reasonable.

Table S2 Selected Fe-N/O bond length (Å), volume cell (Å^3) and octahedral distortion parameters at various temperatures for **1-4**.

	[Fe(qsal-5-OMe)(qsal-I)]NO_3·2MeOH **1**		[Fe(qsal-5-OMe)(qsal-I)]NCS MeOH·H_2O **2**
	150 K	**300 K**	**150 K**
Fe1-O1ph	1.868(4)	1.918(4)	1.912(5)
Fe1-O2ph	1.884(4)	1.901(4)	1.898(4)
Fe1-Oph$_{av}$	1.876	1.910	1.900
Fe1-N1quin	2.026(4)	2.113(4)	2.158(4)
Fe1-N2im	1.988(5)	2.088(4)	2.117(5)
Fe1-N3quin	2.026(4)	2.135(4)	2.167(4)
Fe1-N4im	1.984(5)	2.078(5)	2.127(5)
Fe1-N$_{av}$	2.006	2.103	2.142
V / Å^3	1644	1687	1634
Σ-Fe1, Fe2	43	60	71
Θ-Fe1, Fe2	126	213	272
Spin State	LS	HS	HS

	[Fe(qsal-5-OMe)(qsal-I)]BF_4·MeOH **3**		[Fe(qsal-5-OMe)(qsal-I)]OTf·MeOH **4**	
	150 K	**300 K**	**150 K**	**280 K**
Fe1-O1ph	1.872(2)	1.889(2)	1.880(4)	1.900(4)
Fe1-O2ph	1.878(2)	1.898(2)	1.877(3)	1.908(3)
Fe1-Oph_{av}	1.875	1.894	1.879	1.904
Fe1-N1quin	1.982(3)	2.115(2)	1.980(5)	2.130(4)
Fe1-N2im	1.961(2)	2.059(3)	1.949(6)	2.086(5)
Fe1-N3quin	1.969(2)	2.092(2)	1.977(3)	2.122(4)
Fe1-N4im	1.937(2)	2.057(2)	1.945(7)	2.093(5)
Fe1-N_{av}	1.962	2.081	1.962	2.107
V / $Å^3$	1606	1649	1679	1739
Σ-Fe1, Fe2	48	58	46	58
Θ-Fe1, Fe2	124	190	118	213
Spin state	LS	HS	LS	HS

Table S3 Crystallographic data and structure refinement for **1-4**.

	[Fe(qsal-5-OMe)(qsal-I)]NO_3·2MeOH **1**		[Fe(qsal-5-OMe)(qsal-I)]NCS·MeOH·H_2O **2**
	150 K	**300 K**	**150 K**
Empirical formula	$C_{33}H_{23}N_5O_6FeI$	$C_{33}H_{23}N_5O_6FeI$	$C_{35}H_{29}FeIN_5O_5S$
Formula weight/ gmol^{-1}	768.31	768.31	814.44
Crystal system	triclinic	triclinic	triclinic
Space group	$P\bar{1}$	$P\bar{1}$	$P\bar{1}$
a / Å	12.0122(3)	11.9974(7)	10.7785(3)
b / Å	12.2552(2)	12.4166(6)	12.6165(4)
c / Å	12.7554(2)	12.9275(5)	13.9032(5)
α / °	80.399(2)	79.464(4)	66.070(3)
β / °	69.404(2)	69.435(5)	74.702(3)
γ / °	69.419(2)	69.693(5)	73.722(3)
Cell volume / Å^3	1643.55(6)	1686.90(16)	1634.41(10)
Z	2	2	2
Absorption coefficient / mm^{-1}	11.484	11.283	12.141
Reflections collected	25178	19654	25047
Independent reflections, R_{int}	6004, 0.0966	6143, 0.1093	5964, 0.0836
Max. and min. transmission	0.531/0.062	1/0.127	0.329/0.081
Restrains/parameters	4/479	0/446	22/458
Final R indices [I ≥ 2σ (I)]	0.0648	0.1125	0.0865
R_1, wR_2	0.1773	0.3133	0.2439
CCDC No.	2281918	2281919	2282219

	[Fe(qsal-5-OMe)(qsal-I)]BF_4·MeOH **3**		[Fe(qsal-5-OMe)(qsal-I)]OTf·MeOH **4**	
	150 K	**300 K**	**150 K**	**280 K**
Empirical formula	$C_{34}H_{27}BF_4FeIN_4O_4$	$C_{34}H_{27}BF_4FeIN_4O_4$	$C_{35}H_{27}F_3FeIN_4O_7S$	$C_{35}H_{27}F_3FeIN_4O_7S$
Formula weight/ gmol^{-1}	825.15	825.15	887.41	887.41
Crystal system	triclinic	triclinic	triclinic	triclinic
Space group	$P\bar{1}$	$P\bar{1}$	$P\bar{1}$	$P\bar{1}$
a / Å	10.7366(3)	10.8316(5)	12.2770(4)	11.9334(2)
b / Å	12.3118(2)	12.4983(6)	12.4031(5)	12.6849(2)
c / Å	12.7998(3)	12.8260(8)	12.7647(6)	13.1443(4)
α / °	103.907(2)	104.192(5)	68.856(4)	71.125(2)
β / °	98.433(2)	99.345(4)	86.751(3)	86.434(2)
γ / °	96.219(2)	94.337(4)	68.419(4)	67.786(2)
Cell volume / Å^3	1606.35(7)	1648.87(16)	1679.29(13)	1738.87(7)
Z	2	2	2	2
Absorption coefficient / mm^{-1}	11.917	11.610	12.047	11.634
Reflections collected	24251	24981	25194	27210
Independent reflections, R_{int}	5873, 0.0752	5993, 0.0638	6140, 0.0848	6347
Max. and min. transmission	0.519/0.168	0.584/0.180	0.508/0.038	0.358/0.044
Restrains/parameters	9/463	18/473	3/490	0/481
Final R indices [I ≥ 2σ (I)]	0.0996	0.0905	0.0690	0.0698
R_1, wR_2	0.2821	0.2679	0.1675	0.1971
CCDC No.	2281920	2281921	2281922	2281923

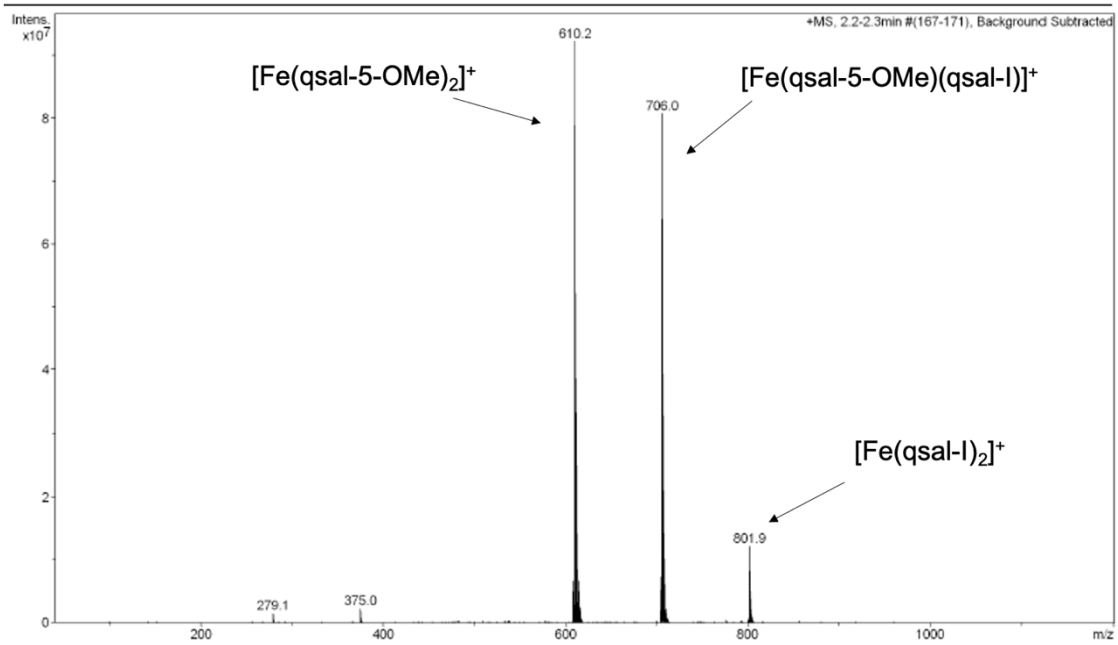

Figure S1. Mass spectrum (ESI^+) for **1-4**.

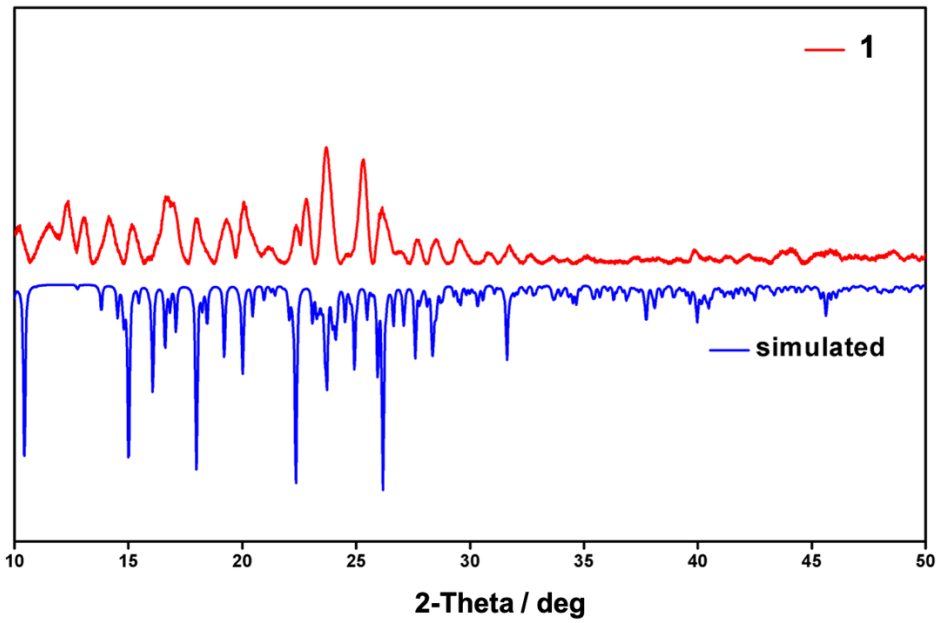

[Fe(qsal-5-OMe)(qsal-I)]NO_3 1.

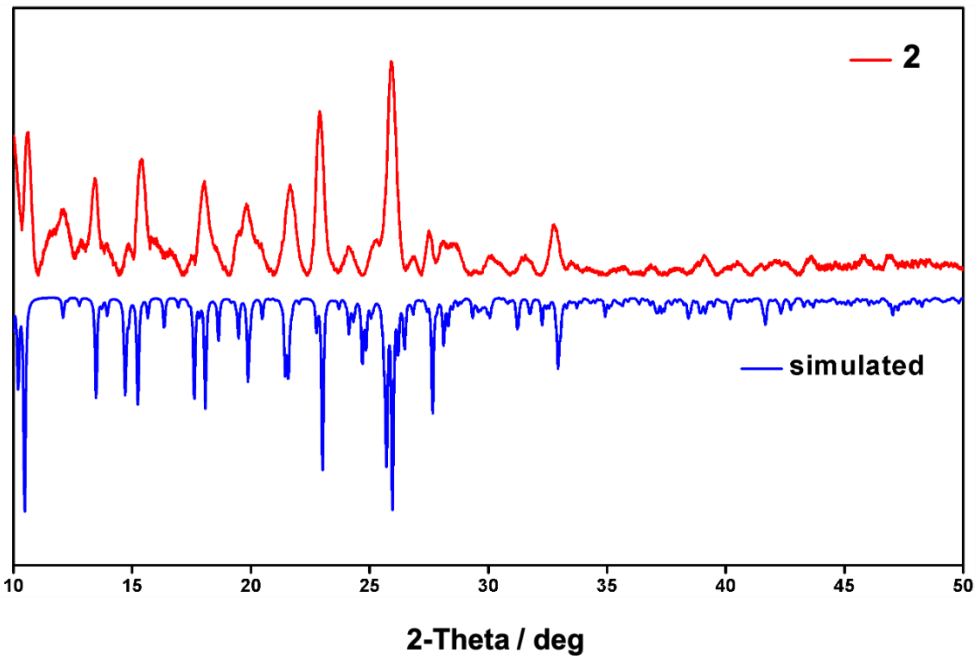

[Fe(qsal-5-OMe)(qsal-I)]NCS 2.

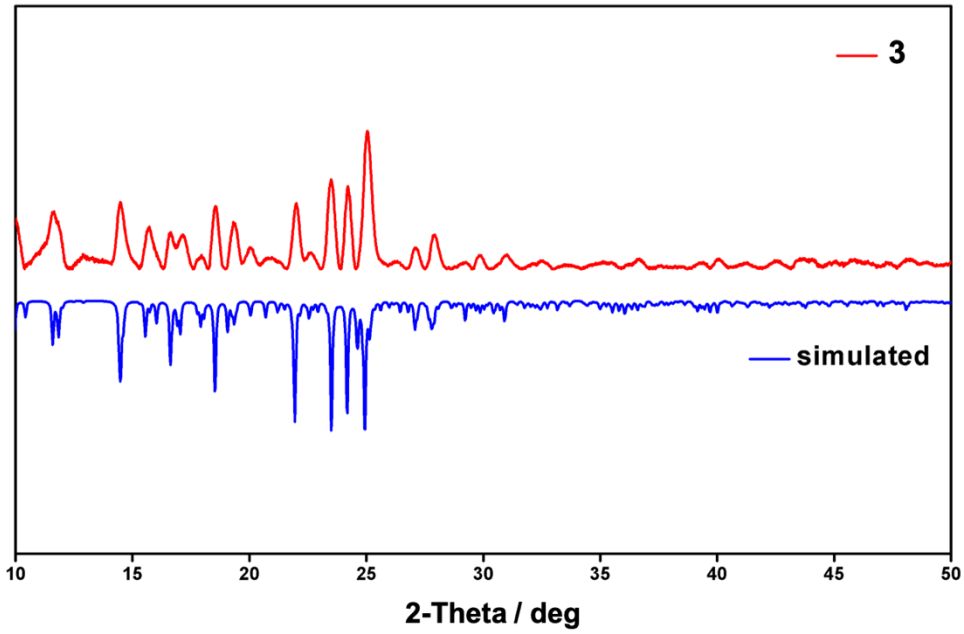

[Fe(qsal-5-OMe)(qsal-I)]BF_4 3.

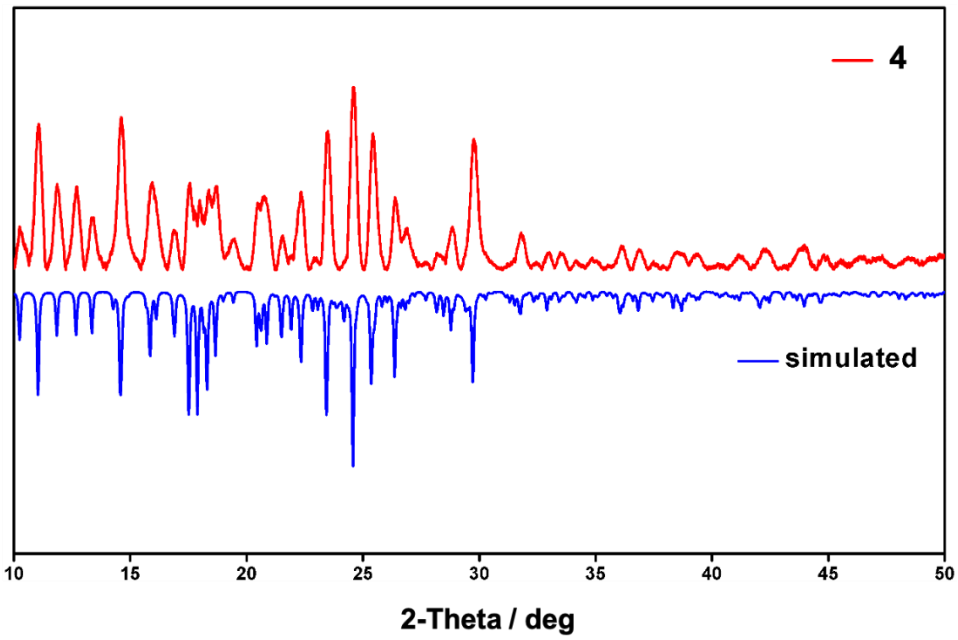

[Fe(qsal-5-OMe)(qsal-I)]OTf 4.

Figure S2 Experimental PXRD diffractograms (blue) and the corresponding simulated patterns (red) for **1-4**.

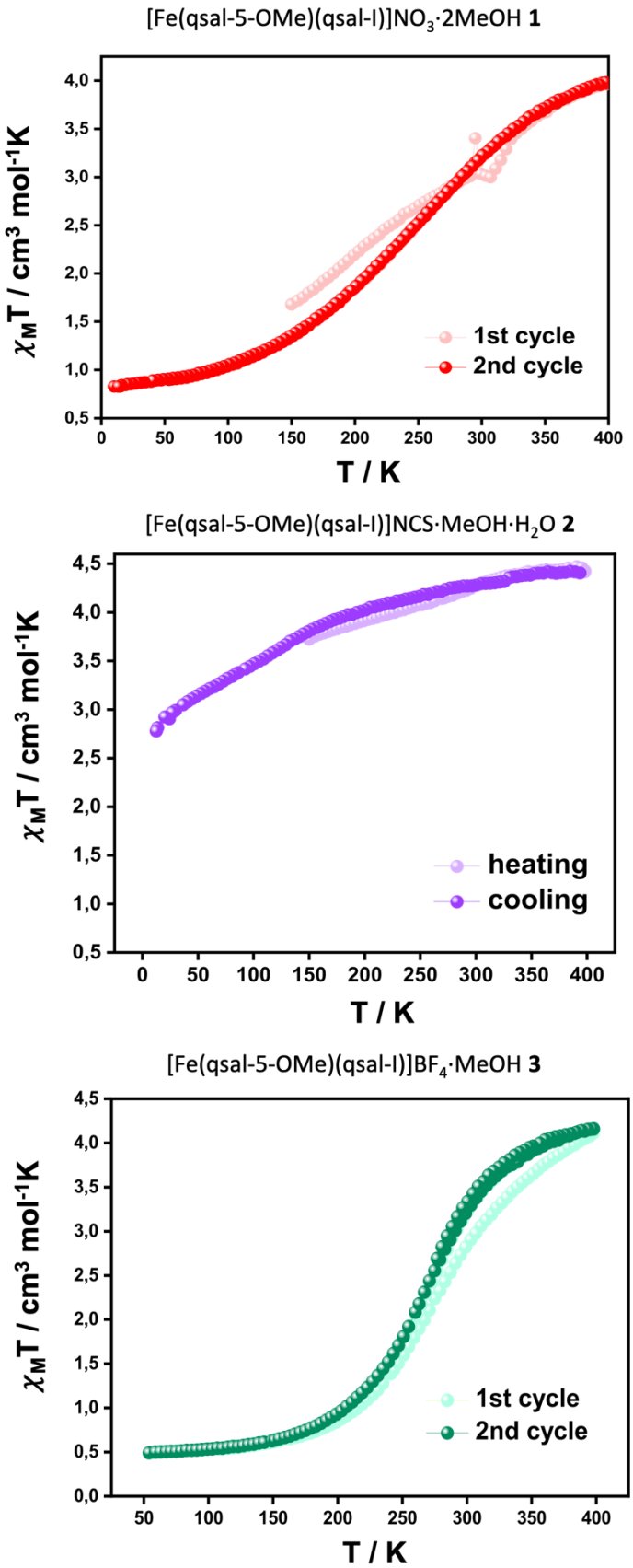

Figure S3 Additional cycles $\chi_M T$ vs. T plots of **1-3**.

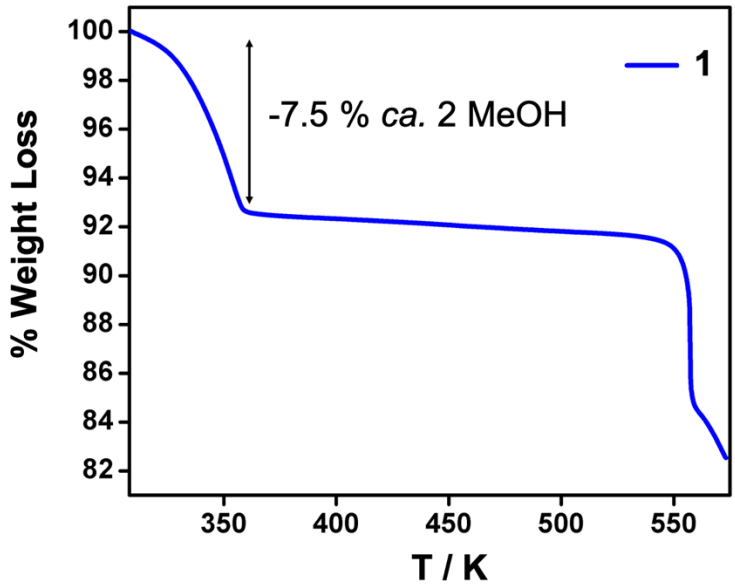
100
98
96
94
92
90
88
86
84
82
% Weight Loss
350
400
450
500
550
T / K
1
-7.5 % ca. 2 MeOH

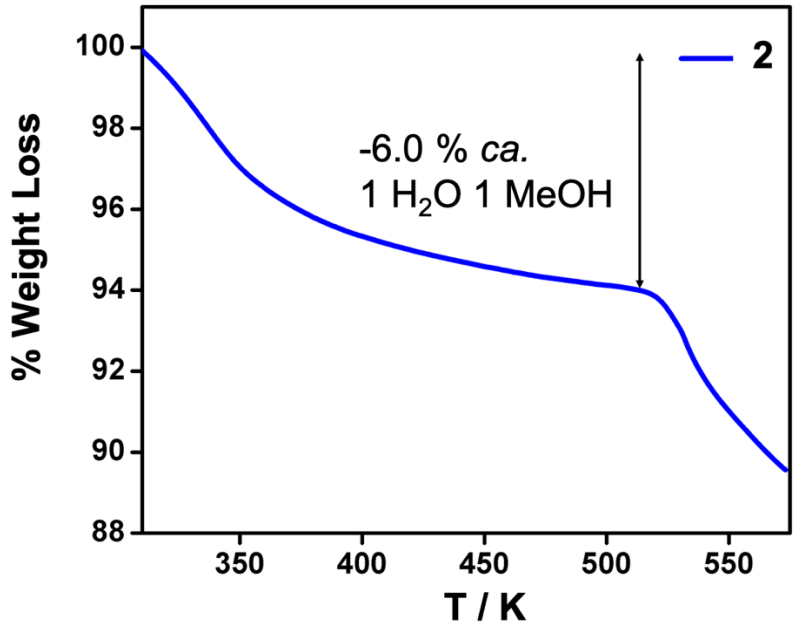
100
98
96
94
92
90
88
% Weight Loss
350
400
450
500
550
T / K
2
-6.0 % ca.
1 H2O 1 MeOH

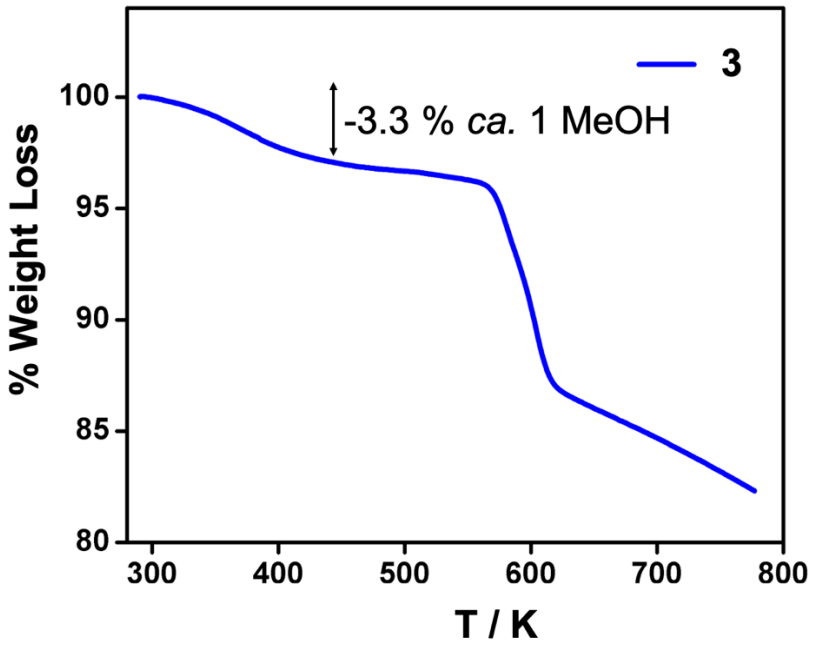

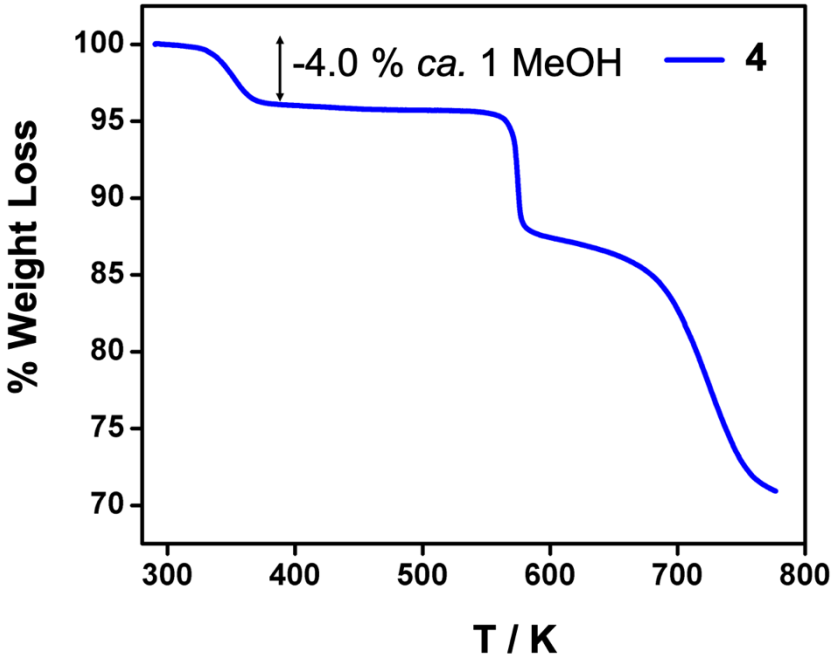

Figure S4 TGA curves for **1-4**.

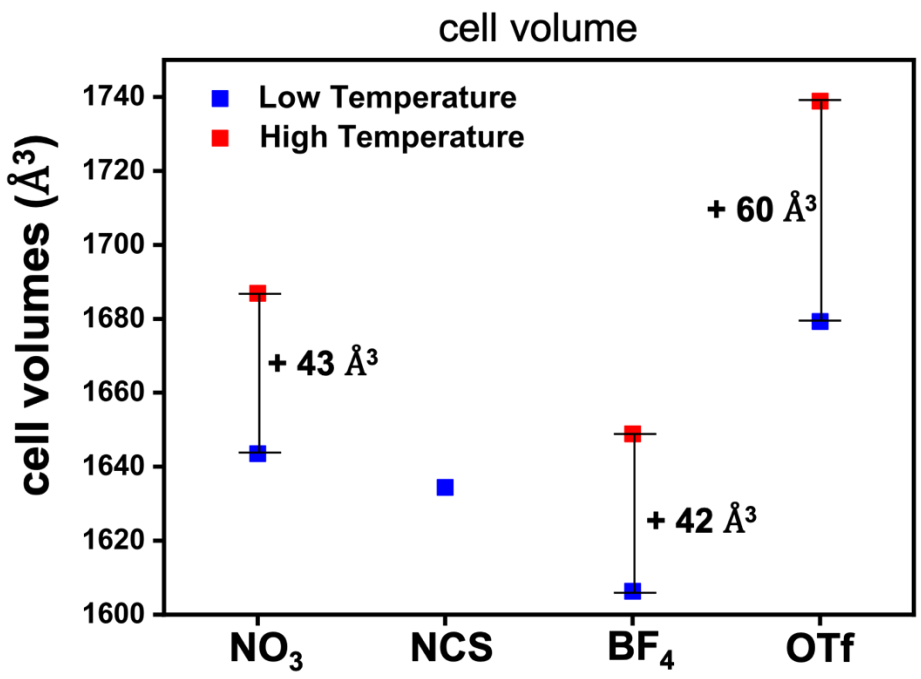

Figure S5: Plot of the variation of the cell volume at low (blue) and high (red) temperature for **1-4.**

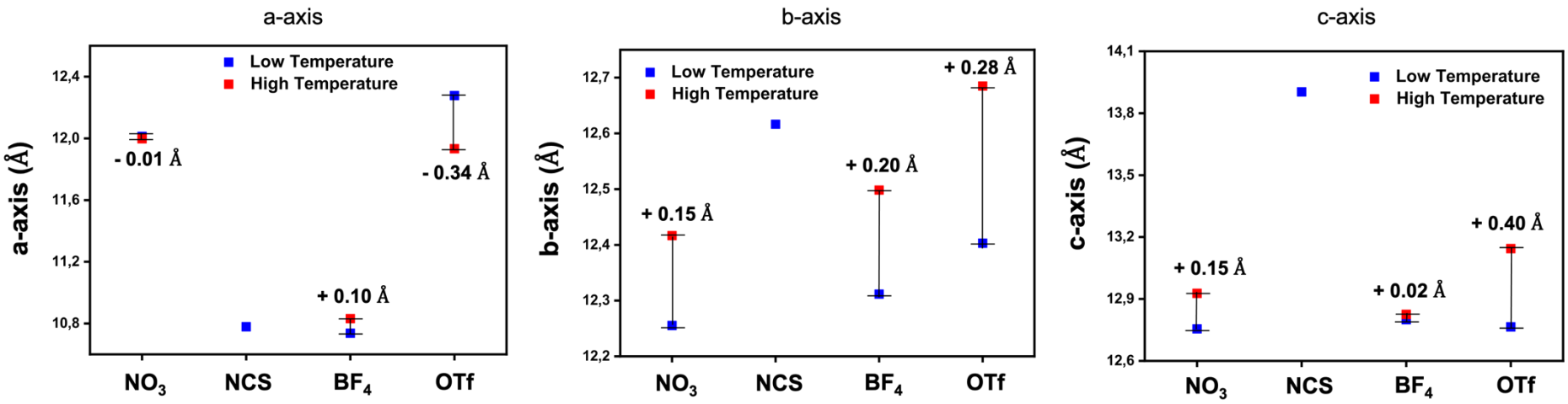

Figure S6: Plot of the variation of the cell parameter a-axis, b-axis and c-axis at low (blue) and high (red) temperature for **1-4.**

Table S4 Intermolecular interactions for **1-4** (Å).

		[Fe(qsal-5-OMe)(qsal-I)]NO_3·2MeOH **1**		[Fe(qsal-5-OMe)(qsal-I)]NCS MeOH·H_2O **2**
		150 K	**300 K**	**150 K**
1D chains				
Fe-Fe				
	π-π (C10-C10)	3.287	3.450	3.444
	π-π (C28-C24)	3.181	3.228	3.388
	C-H···O (H10-O2)	2.640	2.580	-
	$C_{aromatic}$···I (C4-I1)	3.631	3.672	-
	Fe-Fe (Type A)	6.862	6.832	6.785
	Fe-Fe (Type B)	7.226	7.260	8.967
2D plane				
	π-π (P4AE) (C1-C2)	3.361	3.415	3.380
	C-H···π (P4AE) (H3-centr)	2.624	2.672	3.281
	π···O	-	-	3.936
	C-H···C-H	-	-	2.782
3D structure				
	C_{arom}···I (C12-I2)	3.020	-	3.563
	C-H···p	-	-	2.797
Anion	X···CH	-	-	
	O···CH	2.679	3.057	
	S···CH	-	-	
				3.379
Solvent		1.877	3.223	2.794

		[Fe(qsal-5-OMe)(qsal-I)]BF_4·MeOH **3**		[Fe(qsal-5-OMe)(qsal-I)]OTf·MeOH **4**	
		150 K	**300 K**	**150 K**	**280 K**
1D chains					
Fe-Fe					
	π-π (C10-C10)	3.274	3.387	3.260	3.397
	π-π (C28-C24)	3.166	3.226	3.395	3.355
	C-H···O (H10-O2)	2.533	2.552	2.534	2.531
	$C_{aromatic}$···I (C4-I1)	-	-	-	-
	Fe-Fe (Type A)	6.880	6.851	6.796	6.754
	Fe-Fe (Type B)	7.088	7.072	6.980	6.895
2D plane					
	π-π (P4AE) (C1-C2)	-	-	3.404	3.450
	C-H···π (P4AE) (H3-centr)	-	-	2.509	2.559
	C-H···O	-	-	-	-
	O···I	-	-	-	-
3D structure					
	C_{arom}···I (C12-I2)	-	-	-	-
	C-H···π	-	-	-	-
Anion	X···CH	2.512	2.709	-	-
	O···CH	-	-	3.144	3.030
	S···CH	-	-	2.507	2.602
Solvent		3.191	3.137	2.639	2.678

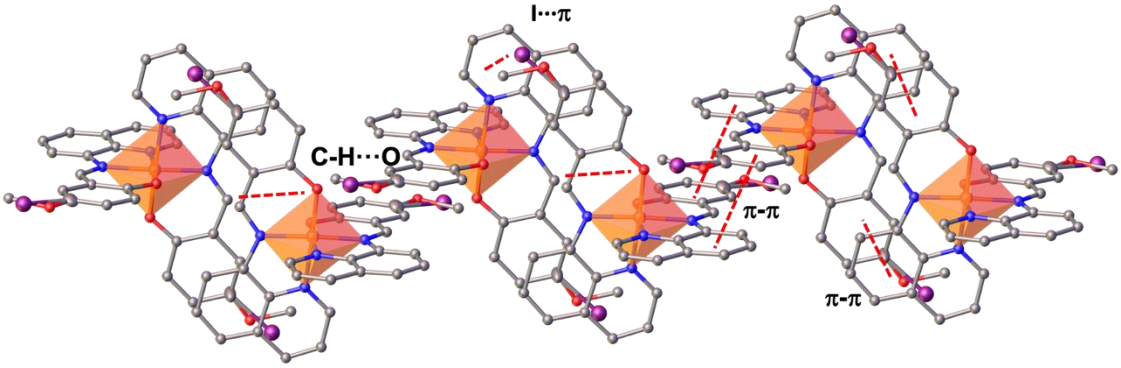

Figure S7: Structural representation of the supramolecular 1D chain for **1** at 150 K.

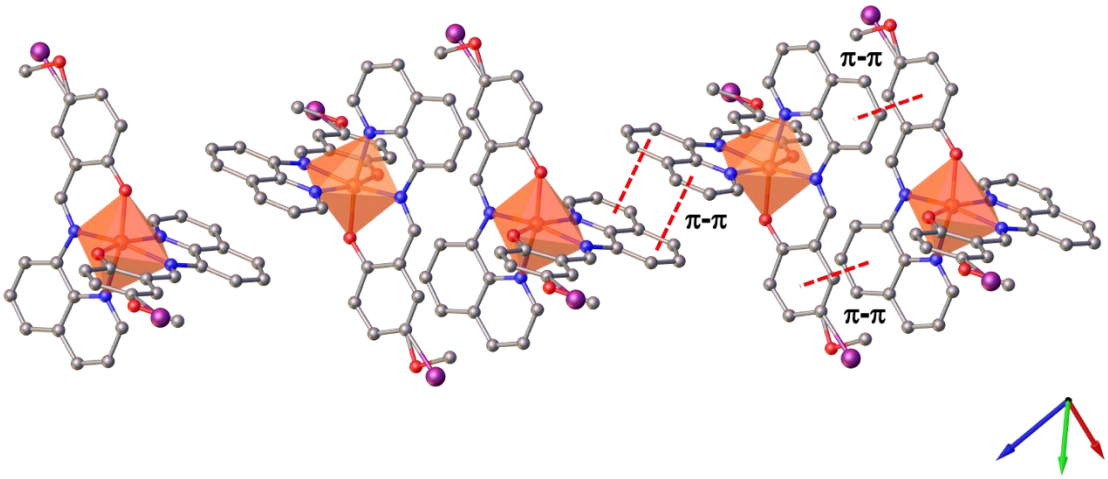

Figure S8: Structural representation of the supramolecular 1D chain for **2** at 150 K.

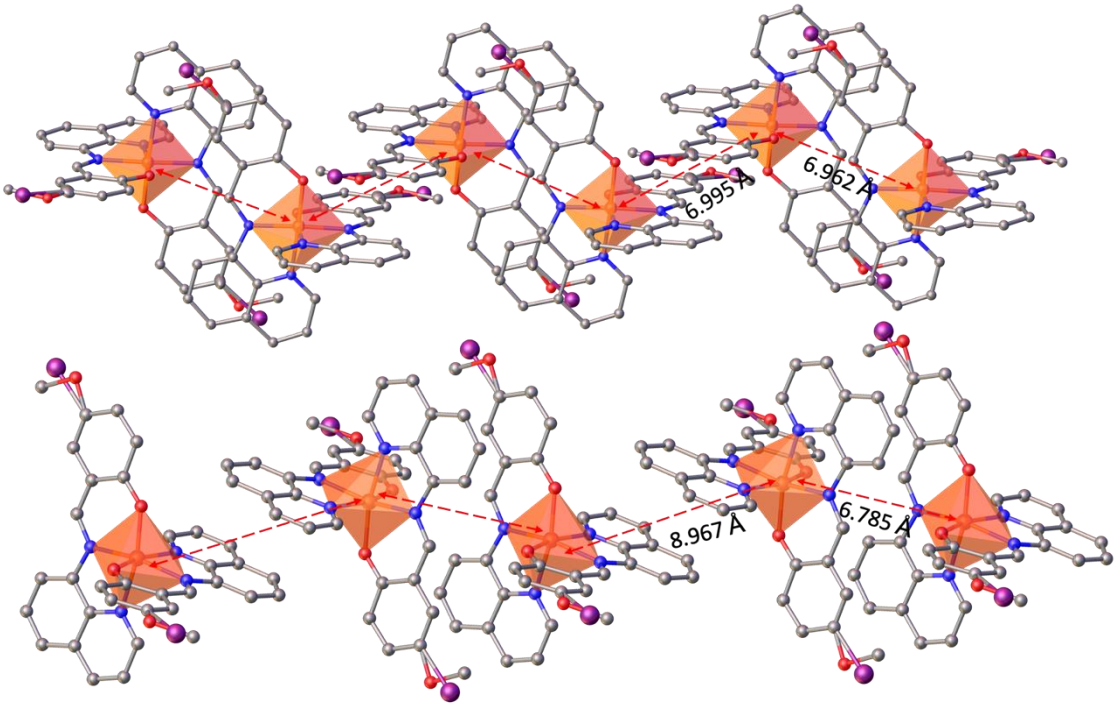

Figure S9: Distance between the metal centers in a 1D chain disposition for **1** (top) and **2** (bottom).

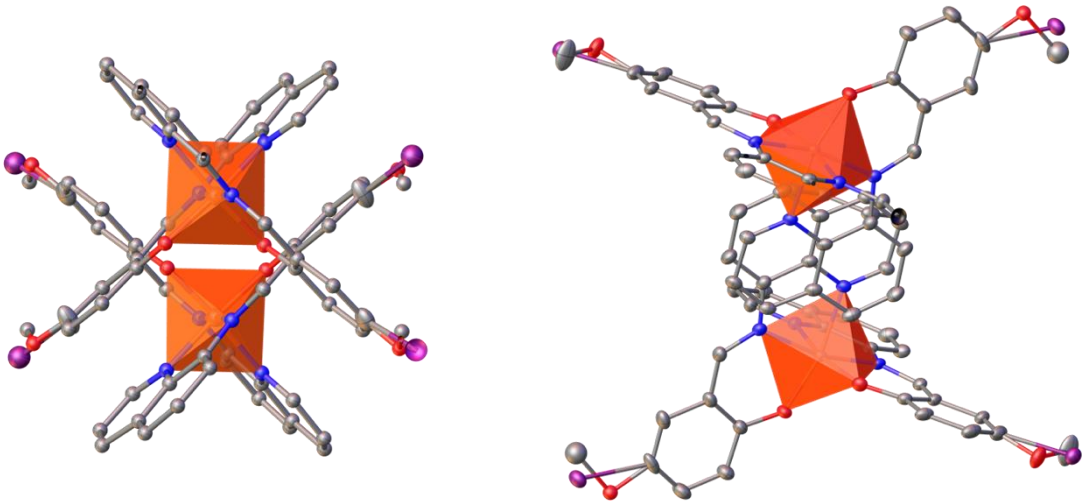

Figure S10: 1D chain cross-section for **1** (left) and **2** (right).

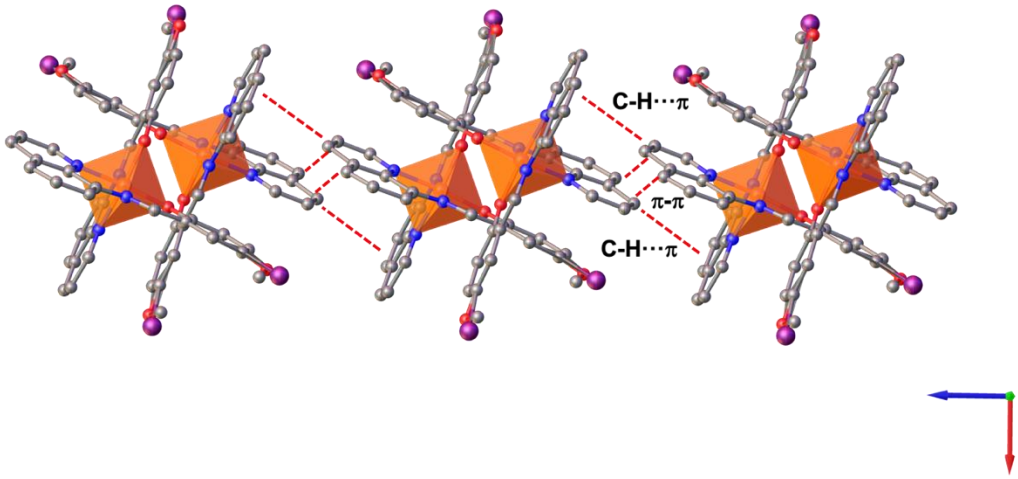

Figure S11: Structural representation of the P4AE interaction in the supramolecular 2D plane of **1** at 150 K.

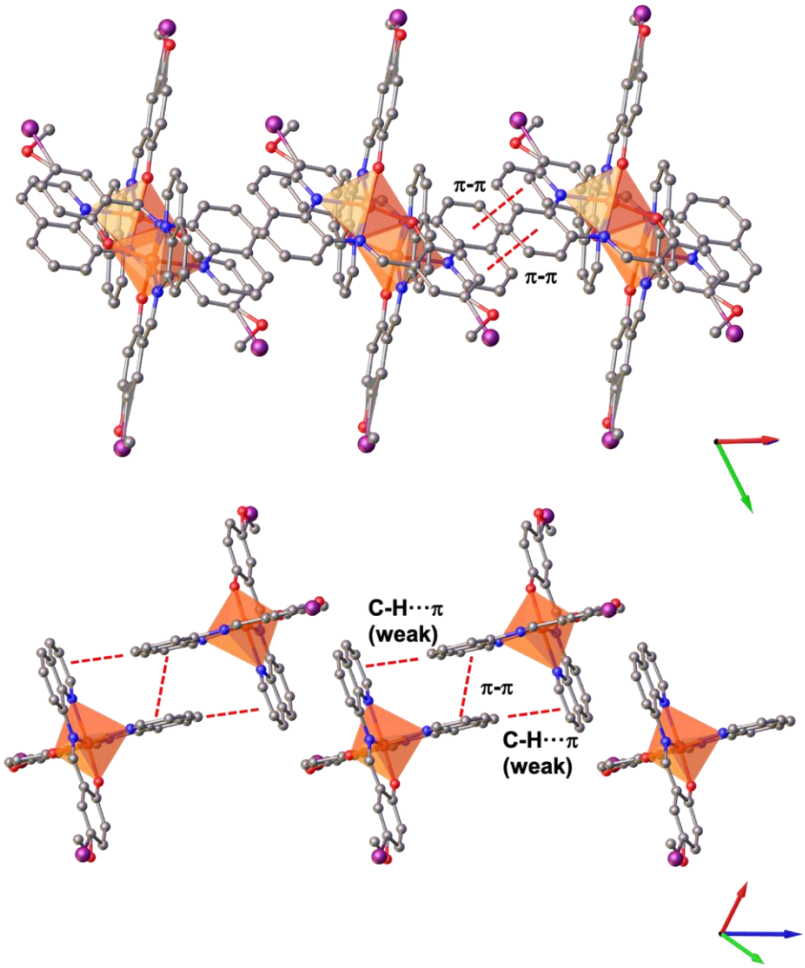

Figure S12: Structural representation from different views of the π-π interactions in the supramolecular 2D plane of **2** at 150 K.

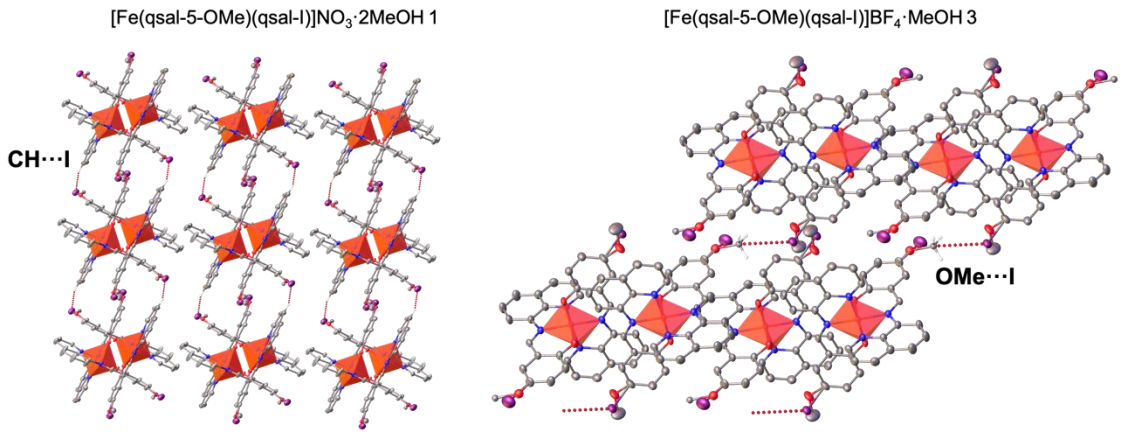

Figure S13: Structural representation of the 3D structure with the cations interacting by C-H···I interactions for **1** (left) and **2** (right).

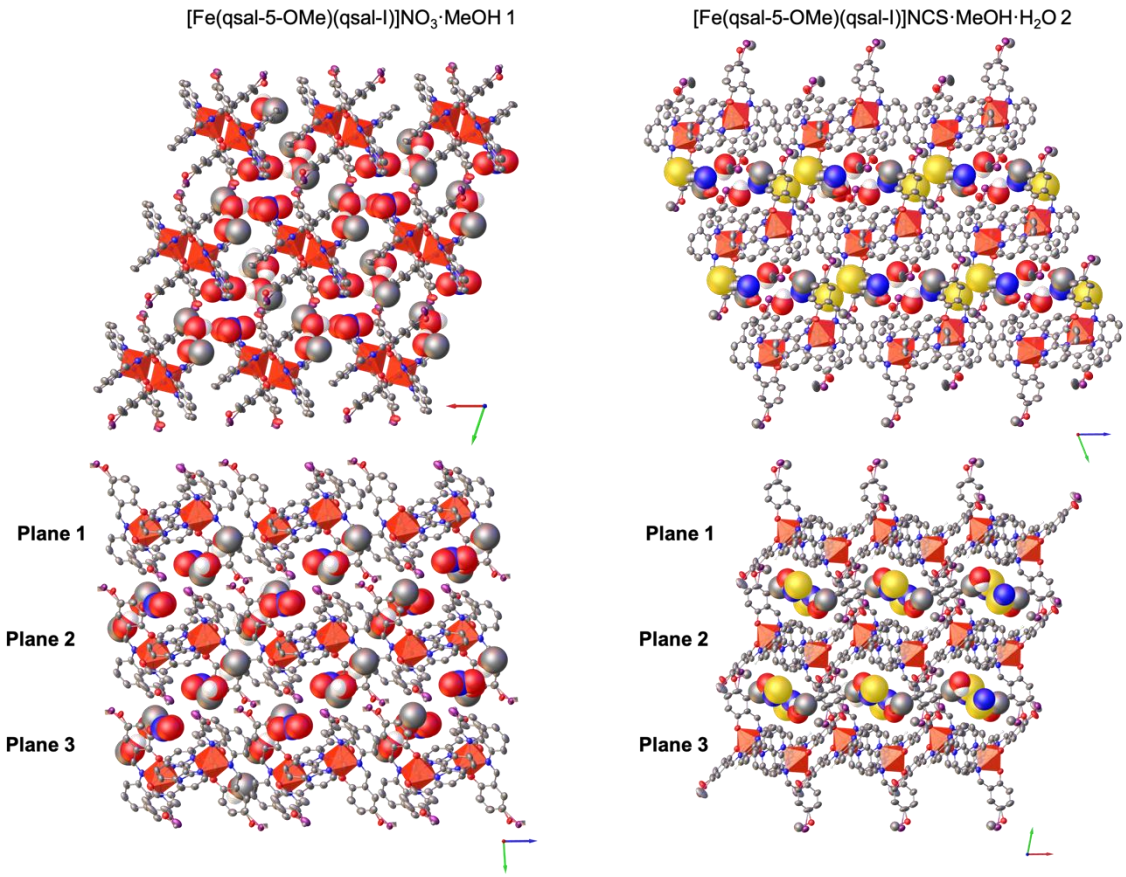

Figure S14: Structural representation of the 3D structure of **1** (left) and **2** (right) at 150 K.

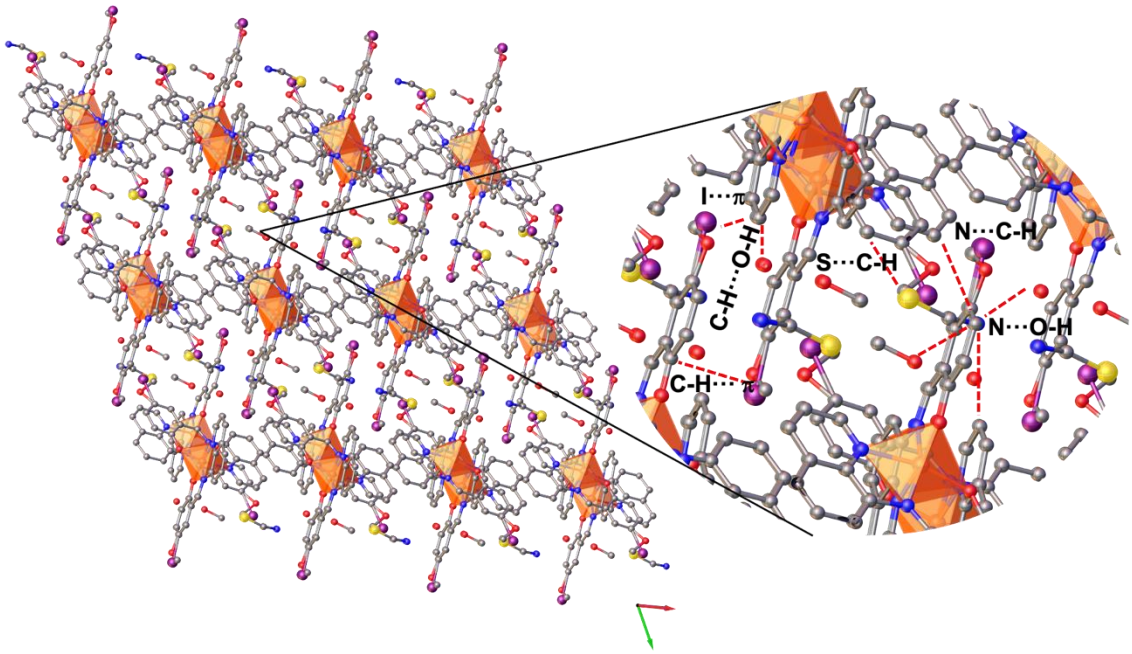

Figure S15: Structural representation of the 3D structure with the interactions of **2** at 150 K.

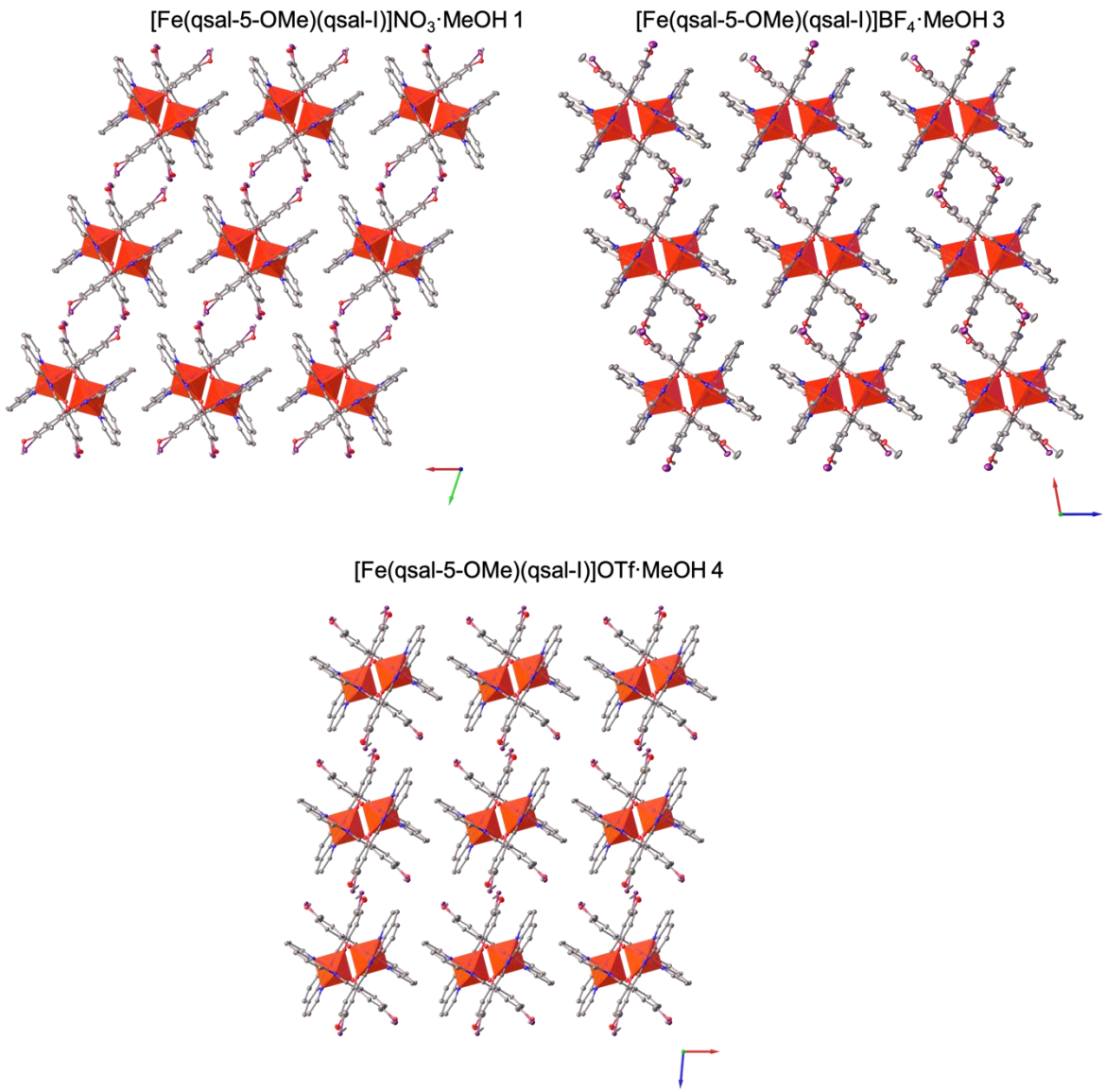

Figure S16: Structural representation of the 3D structure with the methoxy-iodine groups facing each other (**1** and **3**, top) and shifted (**4** bottom).

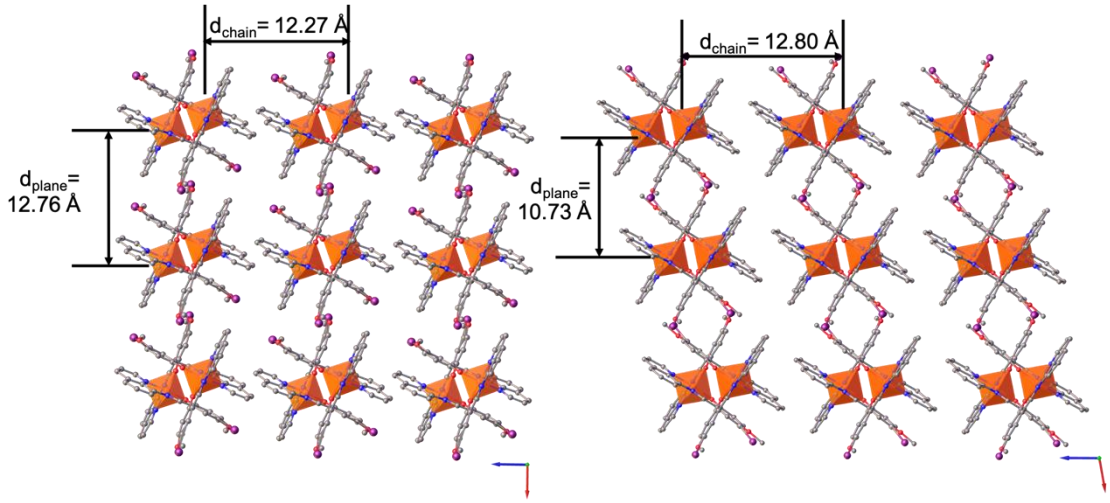

Figure S17: View of d_{chain} (horizontal) and d_{plane} (vertical) of **4** (left) and **3** (right) at 150 K.

Table S5 Distances between the chains (d_{chain}) and the planes (d_{plane}) at different temperatures (LT = low temperature, RT = room temperature, HT = high temperature) for **1-4.**

	T = 150 K		T = 300 K (280 K for **5**)	
	d_{chain}	d_{plane}	d_{chain}	d_{plane}
[Fe(qsal-5-OMe)(qsal-I)]NO_3·2MeOH **1**	12.012	12.255	11.997	12.417
[Fe(qsal-5-OMe)(qsal-I)]NCS·MeOH·H_2O **2**	12.617	10.779		
[Fe(qsal-5-OMe)(qsal-I)]BF_4·MeOH **3**	12.800	10.737	12.826	10.832
[Fe(qsal-5-OMe)(qsal-I)]OTf·MeOH **4**	12.277	12.765	11.933	13.144

Table S6 Angle between the 1D chains (θ°) and N-Fe-N angles (θ°) for **1-4**.

	Temperature	Angle between 1D chains (θ°)	N-Fe-N (θ°)
[Fe(qsal-5-OMe)(qsal-I)]NO_3·2MeOH **1**	150 K	0.0	173
	300 K	0.0	169
[Fe(qsal-5-OMe)(qsal-I)]NCS·MeOH·H_2O **2**	150 K	0.0	164
[Fe(qsal-5-OMe)(qsal-I)]BF_4·MeOH **3**	150 K	0.0	176
	300 K	0.0	171
[Fe(qsal-5-OMe)(qsal-I)]OTf·MeOH **4**	150 K	0.1	176
	280 K	0.0	167

Comparison of the [Fe(qsal-I)(qsal-5-OMe)]OTf with the homoleptic complexes

Table S7 Selected Fe-N/O bond length (Å), volume cell (Å^3) and octahedral distortion parameters at various temperatures for **4-6**.

	[Fe(qsal-5-OMe)(qsal-I)]OTf·MeOH **4**		[Fe(qsal-I)$_2$]OTf·MeOH **5**		[Fe(qsal-5-OMe)$_2$]OTf·DCM **6**	
	150 K	**280 K**	**163 K**	**293 K**	**150 K**	**280 K**
Fe1-O1ph	1.880(4)	1.900(4)	1.874(9)	1.906(7)	1.884(2)	1.882(2)
Fe1-O2ph	1.877(3)	1.908(3)	1.878(7)	1.908(6)	1.873(2)	1.873(2)
Fe1-Oph$_{av}$	1.879	1.904	1.876	1.907	1.878	1.877
Fe1-N1quin	1.980(5)	2.130(4)	1.97(1)	2.10(1)	1.973(2)	1.979(2)
Fe1-N2im	1.949(6)	2.086(5)	1.94(1)	2.145(7)	1.943(2)	1.937(3)
Fe1-N3quin	1.977(3)	2.122(4)	2.010(9)	2.157(3)	1.976(2)	1.987(2)
Fe1-N4im	1.945(7)	2.093(5)	1.95(1)	2.10(1)	1.937(3)	1.939(3)
Fe1-N$_{av}$	1.962	2.107	1.967	2.125	1.957	1.960
V / Å^3	1679	1739	1698	1719	1682	1716
Σ-Fe1, Fe2	46	58	44	62	46	45
Θ-Fe1, Fe2	118	213	114	237	118	117
Spin state	LS	HS	LS	HS	LS	LS

Table S8 Crystallographic data and structure refinement parameters for **4-6**.

	[Fe(qsal-5-OMe)(qsal-I)]OTf·MeOH **4**		[Fe(qsal-I)$_2$]OTf·MeOH **5**		[Fe(qsal-5-OMe)$_2$]OTf·DCM **6**	
	150 K	**280 K**	**163 K**	**293 K**	**150 K**	**280 K**
Empirical formula	$C_{35}H_{27}F_3FeIN_4O_7S$	$C_{35}H_{27}F_3FeIN_4O_7S$	$C_{34}H_{24}F_3FeI_2N_4O_6S$	$C_{34}H_{24}F_3FeI_2N_4O_6S$	$C_{36}H_{28}Cl_2F_3FeN_4O_7S$	$C_{36}H_{28}Cl_2F_3FeN_4O_7S$
Formula weight/ gmol^{-1}	887.41	887.41	982.79	982.79	844.43	844.43
Crystal system	triclinic	triclinic	triclinic	triclinic	triclinic	triclinic
Space group	$P\bar{1}$	$P\bar{1}$	$P\bar{1}$	$P\bar{1}$	$P\bar{1}$	$P\bar{1}$
a / Å	12.2770(4)	11.9334(2)	12.2488(5)	11.7726(4)	12.3329(3)	12.3692(5)
b / Å	12.4031(5)	12.6849(2)	12.3956(4)	12.6918(4)	12.3551(2)	12.4482(4)
c / Å	12.7647(6)	13.1443(4)	12.8192(9)	13.3179(9)	12.8195(3)	12.9361(5)
α / °	68.856(4)	71.125(2)	70.108(5)	69.437(5)	79.960(2)	74.641(3)
β / °	86.751(3)	86.434(2)	87.581(6)	85.020(6)	74.257(2)	80.008(3)
γ / °	68.419(4)	67.786(2)	68.745(5)	67.526(5)	63.718(2)	63.540(4)
Cell volume / Å^3	1679.29(13)	1738.87(7)	1698.40(15)	1719.03(14)	1682.41(7)	1715.93(13)
Z	2	2	2	2	2	2
Absorption coefficient / mm^{-1}	12.047	11.634	19.012	18.784	6.303	6.180
Reflections collected	25194	27210	19123	21734	26061	27182
Independent reflections, R_{int}	6140, 0.0848	6347	6290, 0.0875	4843/0.0681	6166/0.0523	6272/0.0437
Max. and min. transmission	0.508/0.038	0.358/0.044	1.0/0.57	1.0/0.34	0.852/0.502	0.831/0.370
Restrains/parameters	3/490	0/481	6/462	12/462	0/489	0/489
Final R indices [I ≥ 2σ (I)]	0.0690	0.0698	0.0969	0.0715	0.0493	0.0539
R_1, wR_2	0.1675	0.1971	0.3147	0.2346	0.1321	0.1507
CCDC No.	2281922	2281923	929013	929014	2281924	2281925

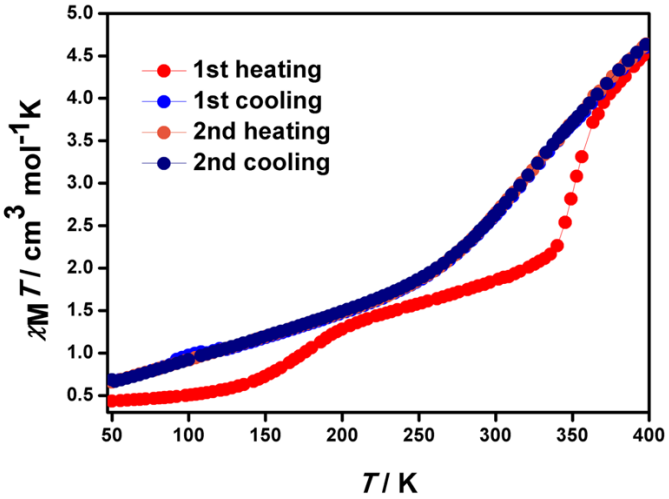

Figure S18: $\chi_M T$ vs. T plot of **6**.

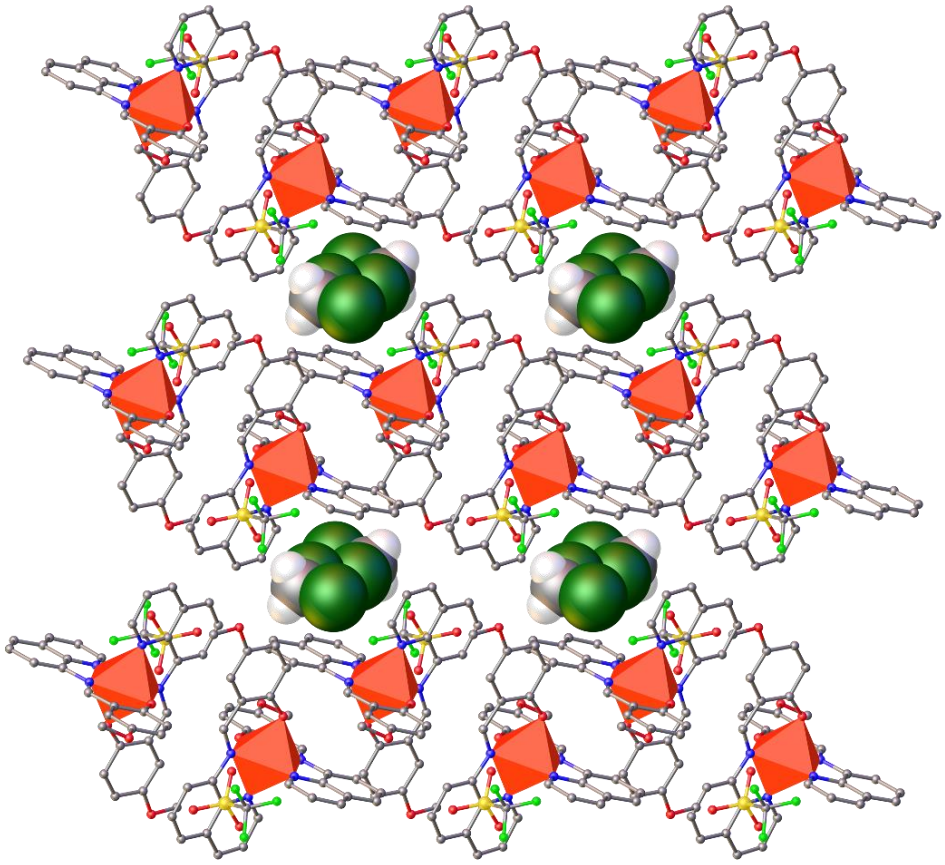

Figure S19: Structural representation of the channel in the 3D structure where the DCM solvent is located for **6**.

Table S9 Intermolecular interactions for **4-6** (Å).

		[Fe(qsal-5-OMe)(qsal-I)]OTf·MeOH **4**		[Fe(qsal-I)$_2$]OTf·MeOH **5**		[Fe(qsal-5-OMe)$_2$]OTf·DCM **6**	
		150 K	**280 K**	**163 K**	**293 K**	**150 K**	**280 K**
1D chains							
Fe-Fe							
	π-π (C10-C10)	3.260	3.397	3.332	3.461	3.282	3.363
	π-π (C28-C24)	3.395	3.355	3.385	3.482	3.462	3.481
	C-H···O (H10-O2)	2.534	2.531	2.506	2.601	2.638	2.656
	Fe-Fe (Type A)	6.796	6.754	6.756	6.643	6.880	6.911
	Fe-Fe (Type B)	6.980	6.895	6.997	6.799	6.957	6.963
2D plane							
	π-π (P4AE) (C1-C2)	3.404	3.450	3.455	3.529	-	-
	C-H···π (P4AE) (H3-cg)	2.509	2.559	2.467	2.569	-	-
	C-H···O	-	-	-	-	-	-
	O···I	-	-	-	-	-	-
3D structure							
	C_{arom}···I (C12-I2)	-	-	-	-	-	-
	C-H···π	-	-	-	-	2.895	2.871
Anion							
	O···CH	2.559	2.642	2.545	2.474	2.494	2.529
	S···CH	2.507	2.602	2.485	2.629	-	-
Solvent		2.639	2.678	2.612	2.586	2.284	2.257

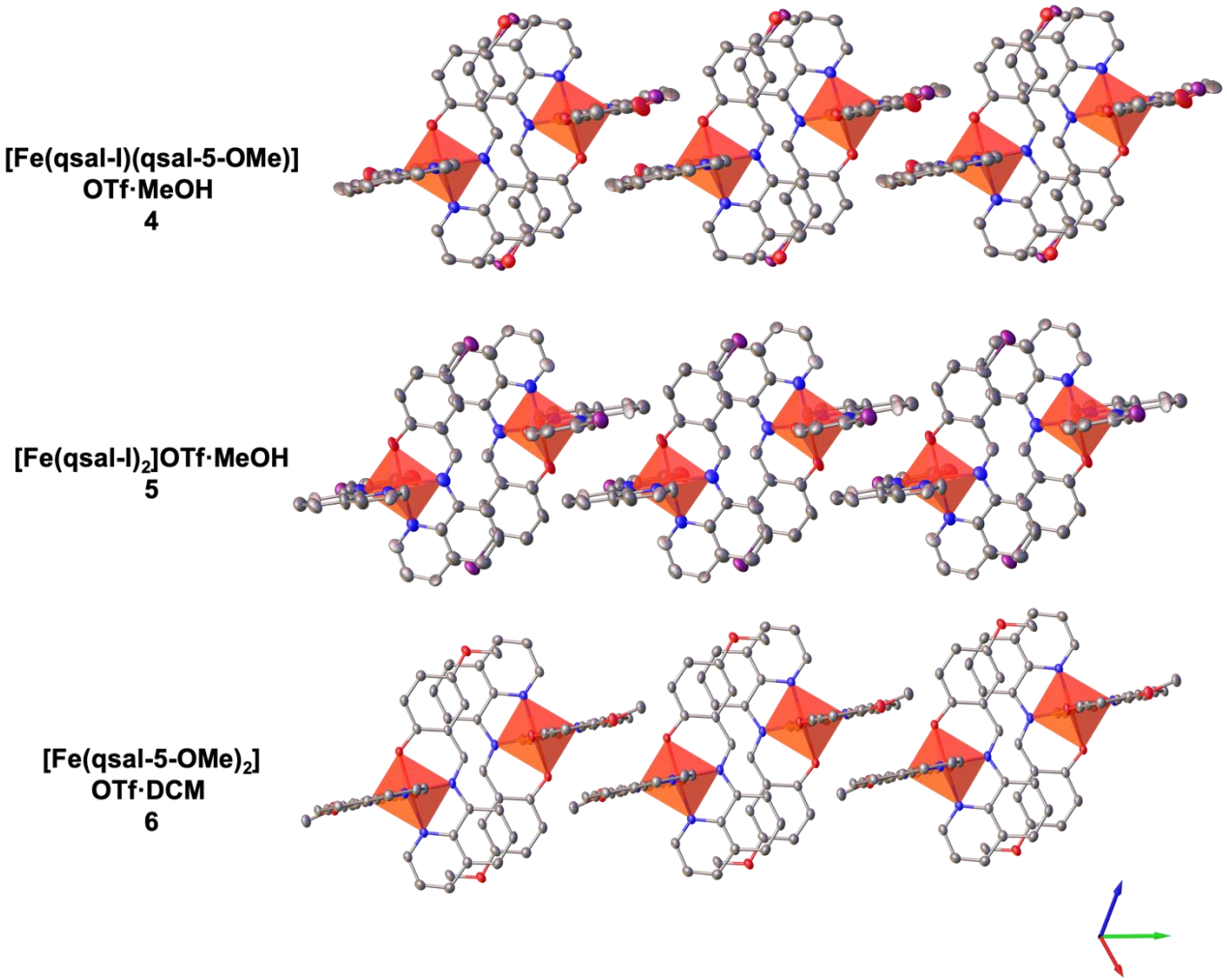

Figure S20: Structural representation of the supramolecular 1D chain for **4**-**6** at 150 K.

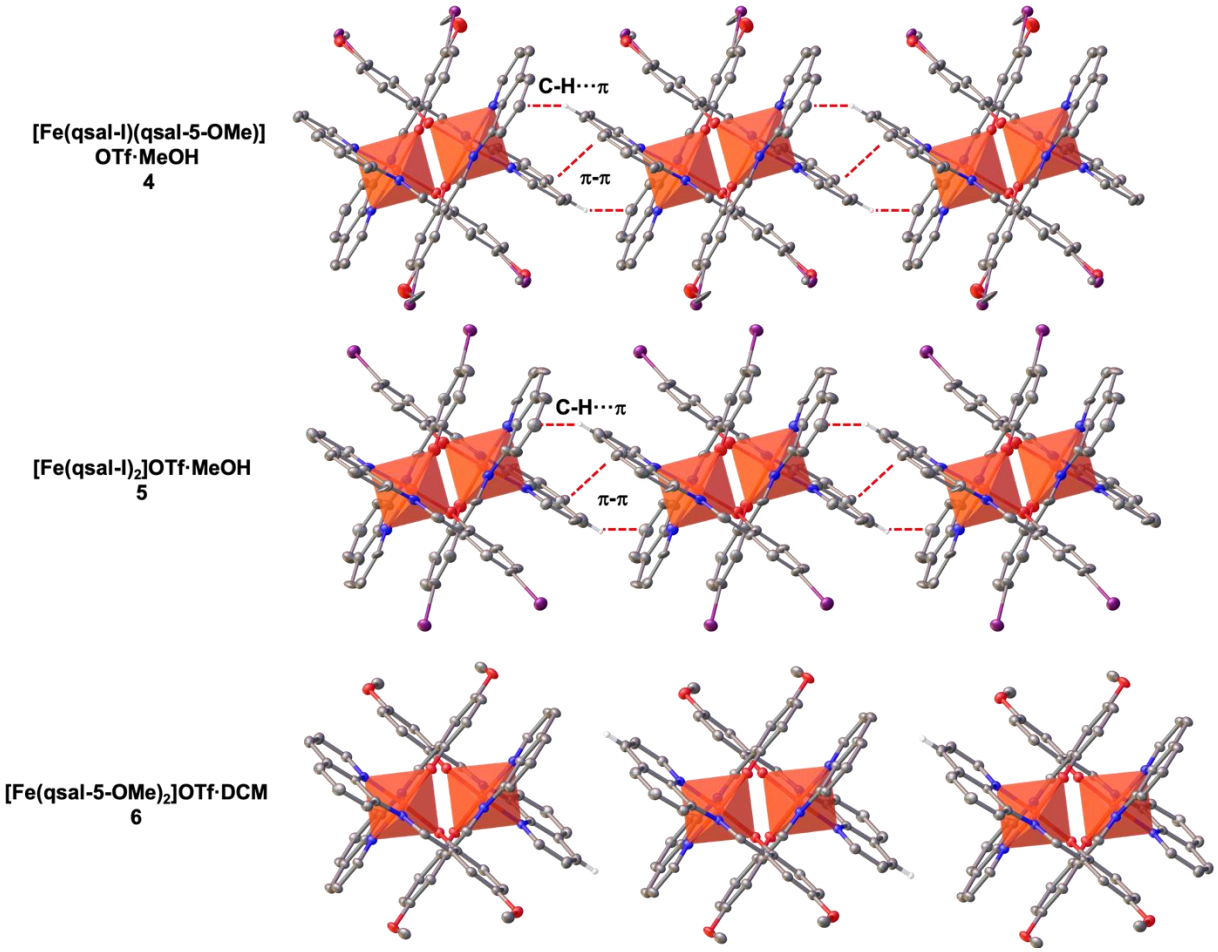

Figure S21: Structural representation of the supramolecular 2D plane for **4**-**6** at 150 K.

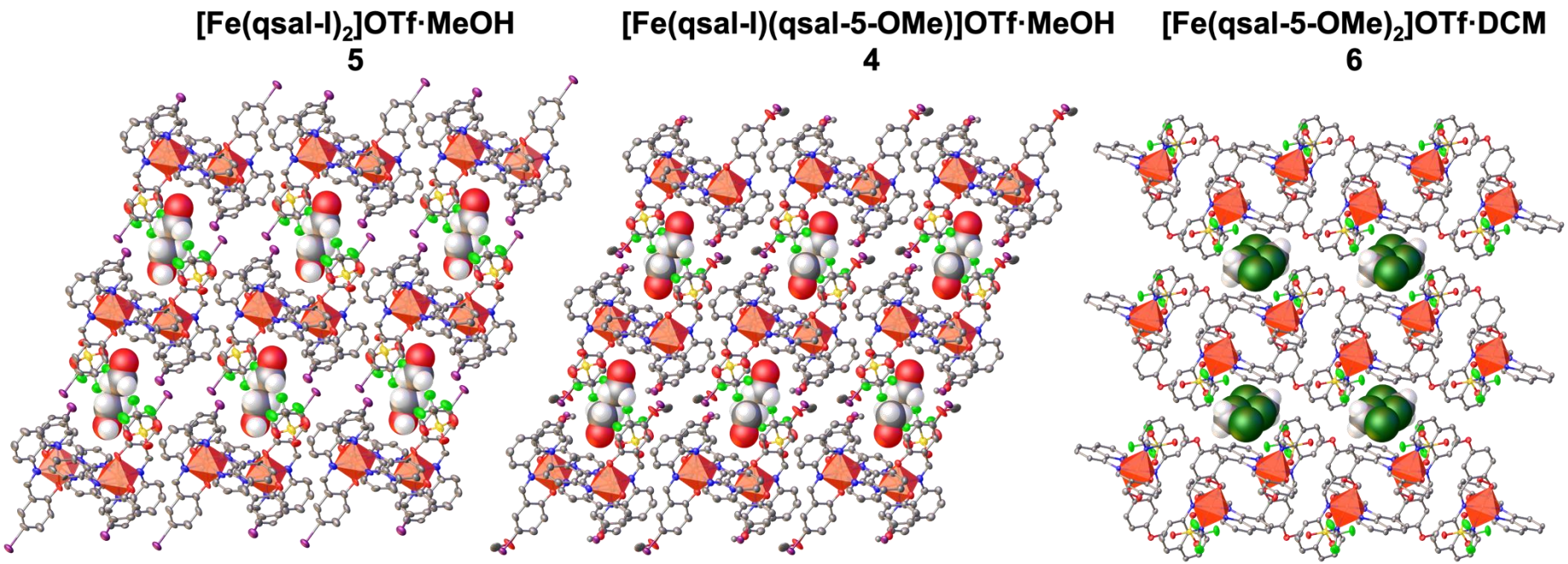

Figure S22: Structural representation of the 3D structure for **4-6** at 150 K.

Table S10: Distances between the chains (d_{chain}) and the planes (d_{plane}) at different temperatures (LT = low temperature, RT = room temperature, HT = high temperature) for **4-6**.

	T = 150 K		T = RT	
	d_{chain}	d_{plane}	d_{chain}	d_{plane}
[Fe(qsal-5-OMe)(qsal-I)]OTf·MeOH **4**	12.277	12.765	11.933	13.144
[Fe(qsal-I)$_2$]OTf·MeOH **5**	12.249	12.819	11.773	13.318
[Fe(qsal-5-OMe)$_2$]OTf·DCM **6**	12.819	12.333	12.936	12.448

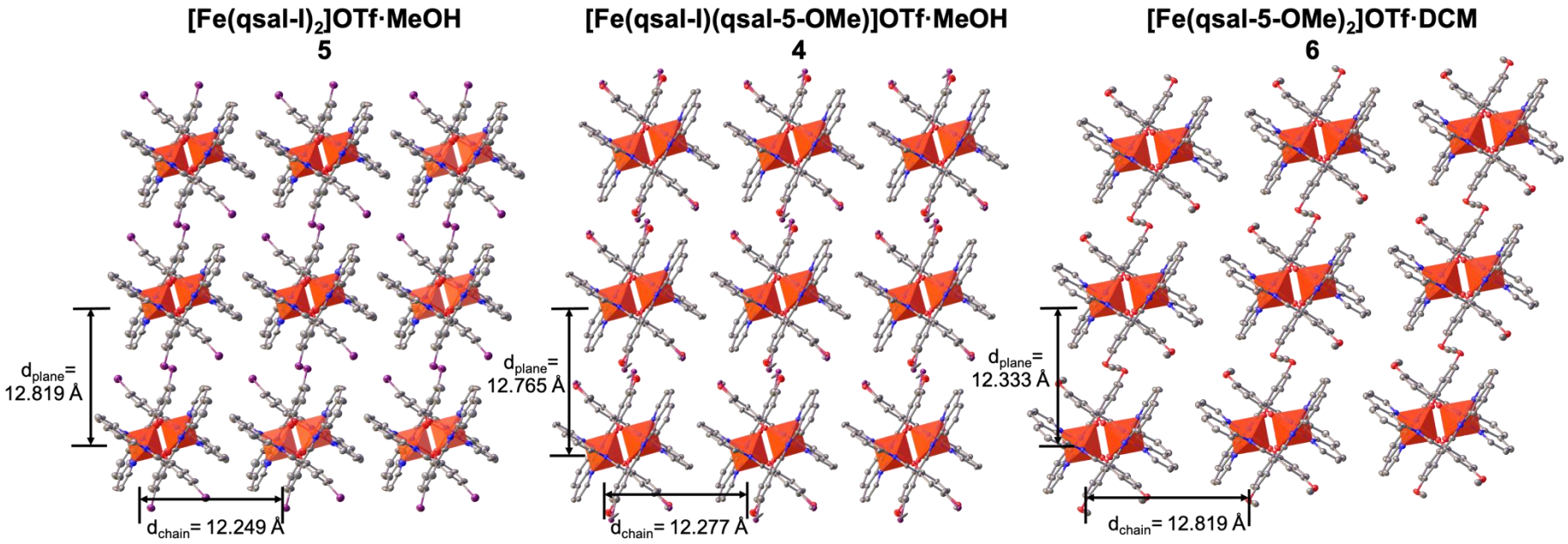

Figure S23: View of d_{chain} (horizontal) and d_{plane} (vertical) for **4-6** at 150 K.

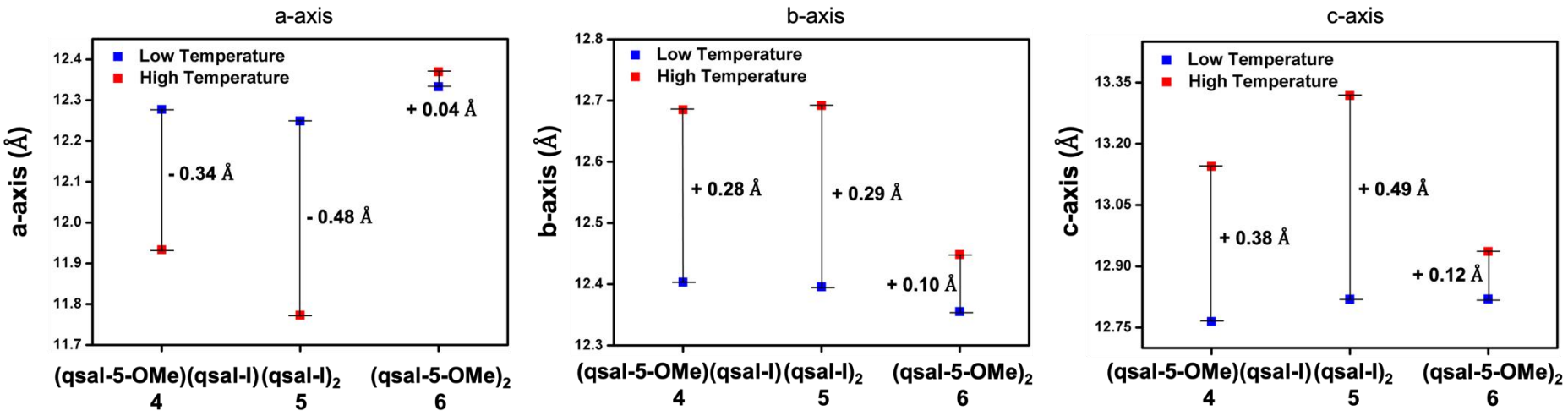

Figure S24: Plot of the variation of the cell parameter *a*-axis, *b*-axis and *c*-axis at low (blue) and high (red) temperature for **4-6.**

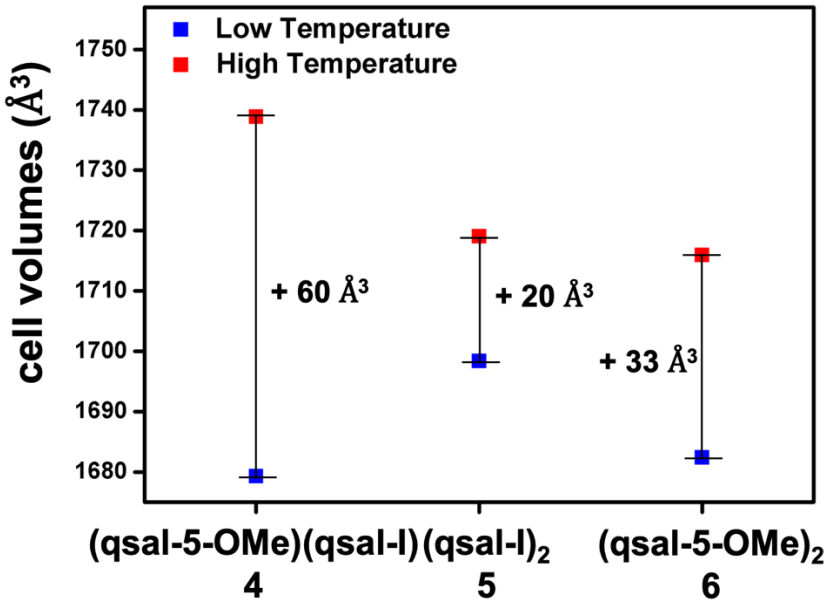

Figure S25: Plot of the variation of the cell volumes at low (blue) and high (red) temperature for **4-6.**

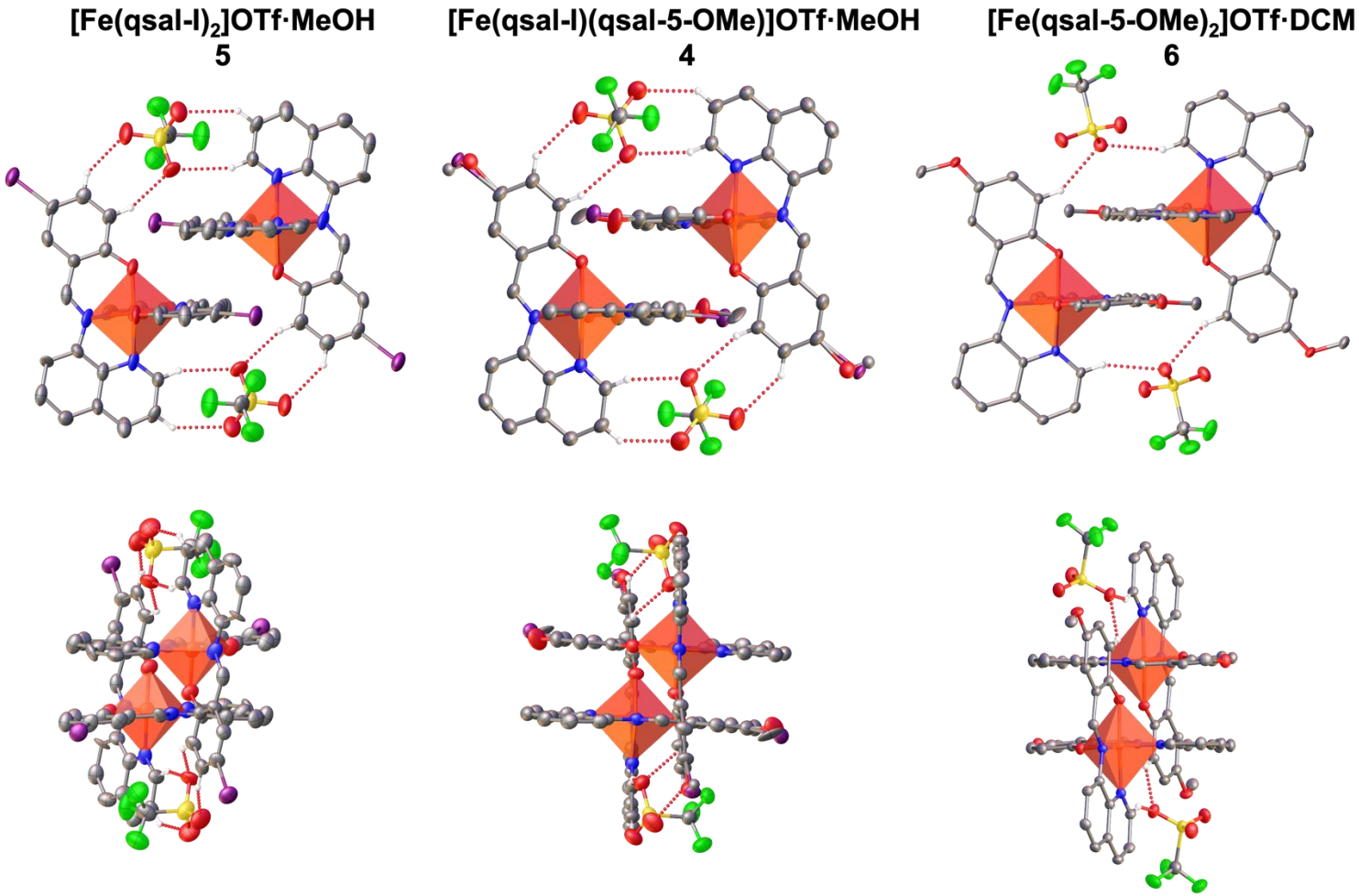

Figure S26: Interactions of the OTf anion within the 1D chain for **4-6** (top). Comparison of the different arrangement of the anion with the 1D chain cross-section for **4-6** (bottom).

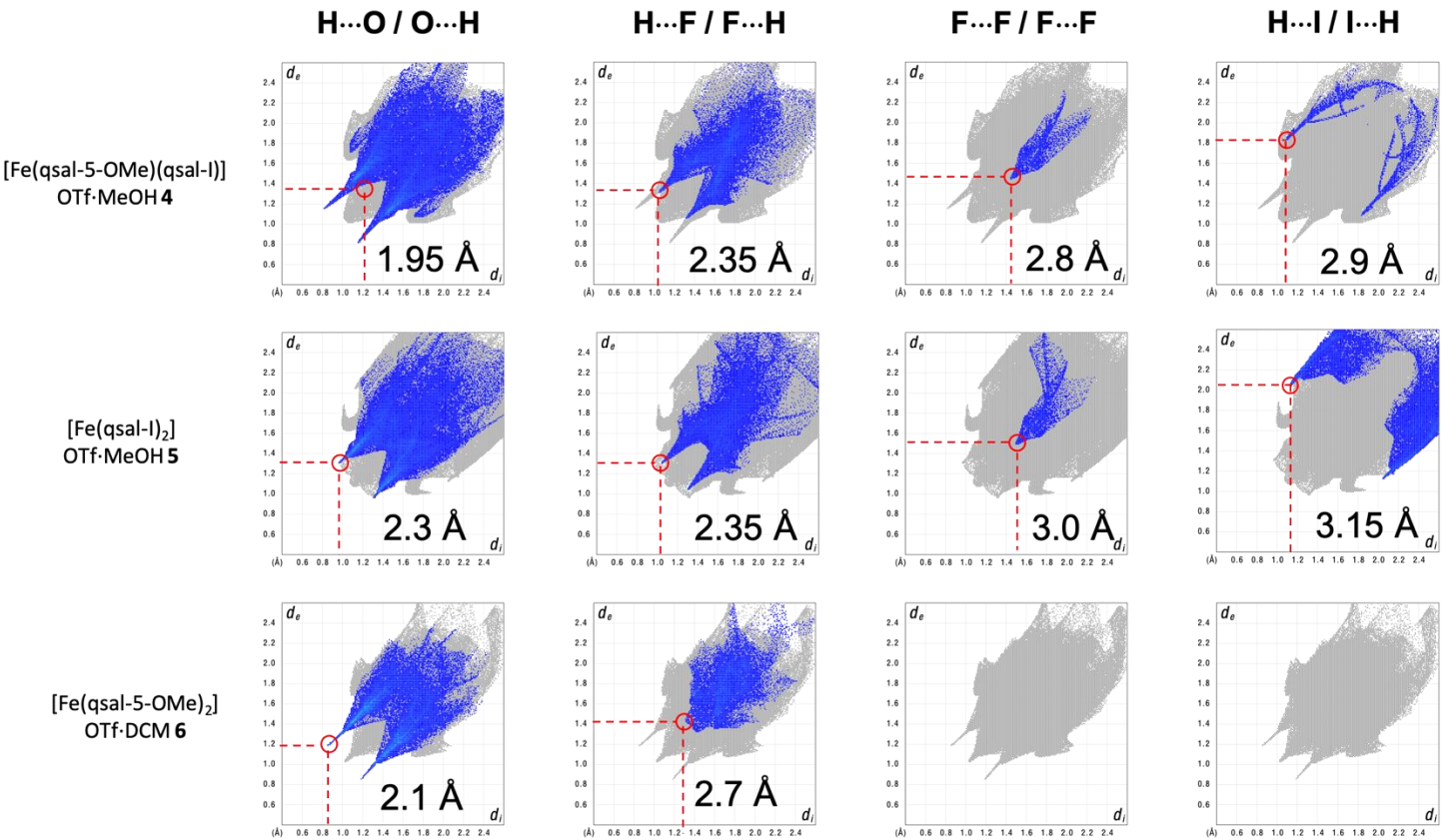

Figure S27: Hirshfeld surface 2D fingerprint plots for **4-6** at 150 K.

Table S11: Intermolecular interactions contributions for **1-6** calculated by Hirshfeld surface at different temperatures.

		H···H	H···C	H···O	H···N	H···I	H···X	H···S	C···C	C···O	C···I	O···F	O···I	I···I	F···F	Other
[Fe(qsal-5-OMe)(qsal-I)]NO_3·2MeOH **1**	150 K															
	300 K	31.0	17.1	20.6	2.6	15.2	-	-	7.3	-	2.9		2.3	0.6	-	0.4
[Fe(qsal-5-OMe)(qsal-I)]NCS·MeOH·H_2O **2**	150 K	38.4	22.5	12.3	8.5	2.6	-	4.6	8.1	1.2	0.3		0.3	0.0	-	1.2
[Fe(qsal-5-OMe)(qsal-I)]BF_4·MeOH **3**	150 K	38.6	21.5	8.7	1.0	1.3	19.1	-	6.3	1.9	1.3		0.0	0.0	0.0	0.3
	300 K	38.0	20.1	9.4	1.4	1.6	19.3	-	6.7	1.8	1.4		0.0	0.0	0.0	0.3
[Fe(qsal-5-OMe)(qsal-I)]OTf·MeOH **4**	150 K	34.8	19.6	21.4	1.5	1.5	11.1	0.0	6.4	1.5	0.9	0.0	0.0	0.0	1.2	0.1
	280 K	35.0	17.8	21.0	2.0	1.3	11.4	0.0	7.4	2.1	0.3		0.1	0.1	1.1	0.4
[Fe(qsal-I)$_2$]OTf·MeOH **5**	163 K	23.3	14.9	19.3	1.3	10.3	10.1	0.0	6.5	1.2	5.8	1.4	0.5	0.8	1.4	4.6
	293 K	24.1	13.3	22.2	1.9	10.5	8.4	0.0	7.3	1.1	4.7		0.7	0.7	1.3	3.8
[Fe(qsal-5-OMe)$_2$]OTf·DCM **6**	150 K	31.3	15.5	19.4	1.0	-	10.3	0.0	5.4	1.6	-	0.9	-	-	0.0	15.5
	280 K	31.6	15.4	19.7	1.0	-	10.5	0.0	5.2	1.5	-		-	-	0.0	15.1

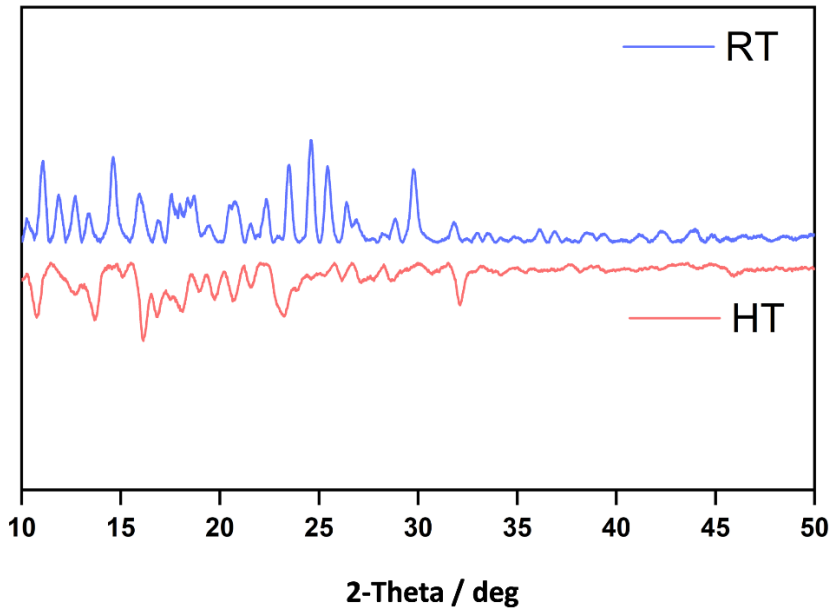

Figure S28: Experimental PXRD diffractograms for **4** at room temperature (blue) and after heating at 400 K (red).

Table S12: Summary of SCO features of the homoleptic and heteroleptic complexes within the family

Compound	SCO	$T_{1/2}$	Hysteresis	Ref
NO_3 anion				
[Fe(qsal-5-OMe)(qsal-I)]NO_3·2MeOH **1**	Gradual	260 K	-	This work
[Fe(qsal-I)$_2$]NO_3·MeOH	Abrupt	210 K	-	[9]
[Fe(qsal-5-OMe)$_2$]NO_3	unknown			-
NCS anion				
[Fe(qsal-5-OMe)(qsal-I)]NCS·MeOH·H_2O **2**	HS	-	-	This work
[Fe(qsal-I)$_2$]NCS·0.25DCM·0.5MeOH	LS	-	-	[10]
[Fe(qsal-5-OMe)$_2$]NCS·DCM	HS	305 K		[11]
BF_4 anion				
[Fe(qsal-5-OMe)(qsal-I)]BF_4·MeOH **3**	Gradual	280 K	-	This work
[Fe(qsal-I)$_2$]BF_4	unknown			-
[Fe(qsal-5-OMe)$_2$]BF_4·MeOH	LS	-		[11]
OTf anion				
[Fe(qsal-5-OMe)(qsal-I)]OTf **4**	Abrupt	$T_{1/2}\uparrow$ = 260 K, $T_{1/2}\downarrow$ = 225 K	35 K	This work
[Fe(qsal-I)$_2$]OTf **5**	Abrupt	$T_{1/2}\uparrow$ = 232 K, $T_{1/2}\downarrow$ = 224 K	8 K	[12]
[Fe(qsal-5-OMe)$_2$]OTf·DCM **6**	Stepped-gradual	T_1 = 160 K, T_2 = 360 K	-	This work

Table S13 Comparison of DFT optimized average metal-ligand bond lengths (Å) and volume cells (Å^3) for the studied systems. The available experimental data is indicated in parenthesis.

		Fe-O_{av}	Fe-N_{av}	volume
[Fe(qsal-5-OMe)(qsal-I)]OTf·MeOH **4**	HS	1.950 (1.904)	2.164 (2.107)	1681 (1739)
	LS	1.910 (1.879)	1.958 (1.962)	1673 (1679)
[Fe(qsal-5-OMe)(qsal-I)]OTf	HS	1.954	2.160	1643
	LS	1.906	1.956	1610
[Fe(qsal-I)$_2$]OTf·MeOH **5**	HS	1.948 (1.907)	2.159 (2.125)	1723 (1719)
	LS	1.907 (1.876)	1.958 (1.962)	1691 (1698)
[Fe(qsal-I)$_2$]OTf	HS	1.955	2.159	1663
	LS	1.910	1.954	1647
[Fe(qsal-5-OMe)$_2$]OTf·DCM **6**	HS	1.950	2.157	1728
	LS	1.904 (1.877)	1.955 (1.957)	1691 (1682)
[Fe(qsal-5-OMe)$_2$]OTf	HS	1.954	2.154	1685
	LS	1.907	1.954	1652

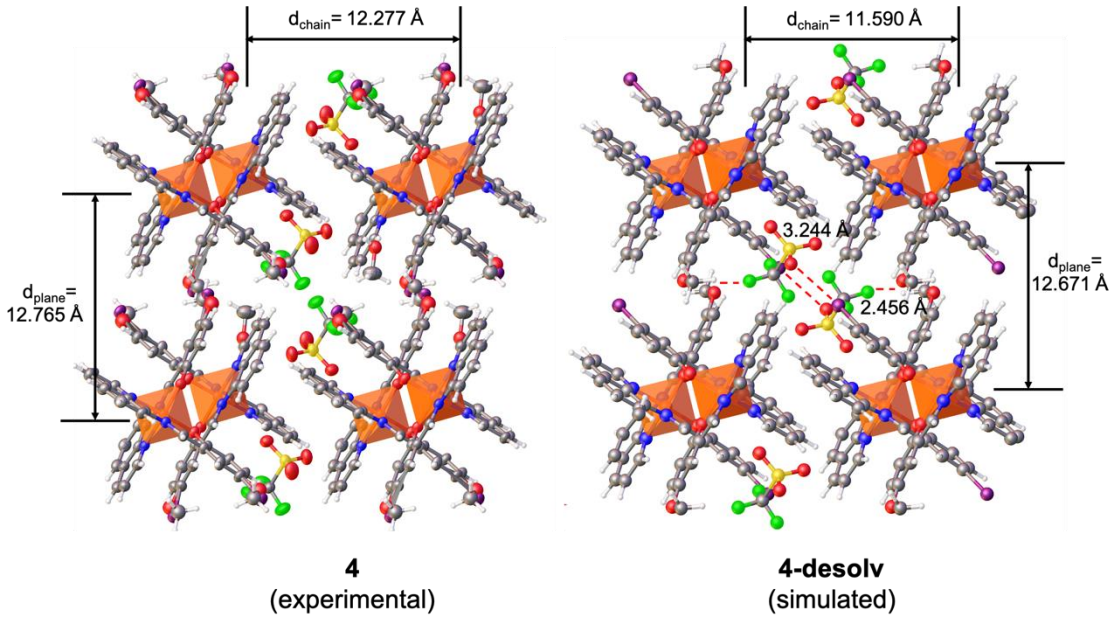

Figure S29: View of d_{chain} (horizontal) and d_{plane} (vertical) and interactions for **4** (experimental) and **4-desolv** (simulated) in the LS state**.**

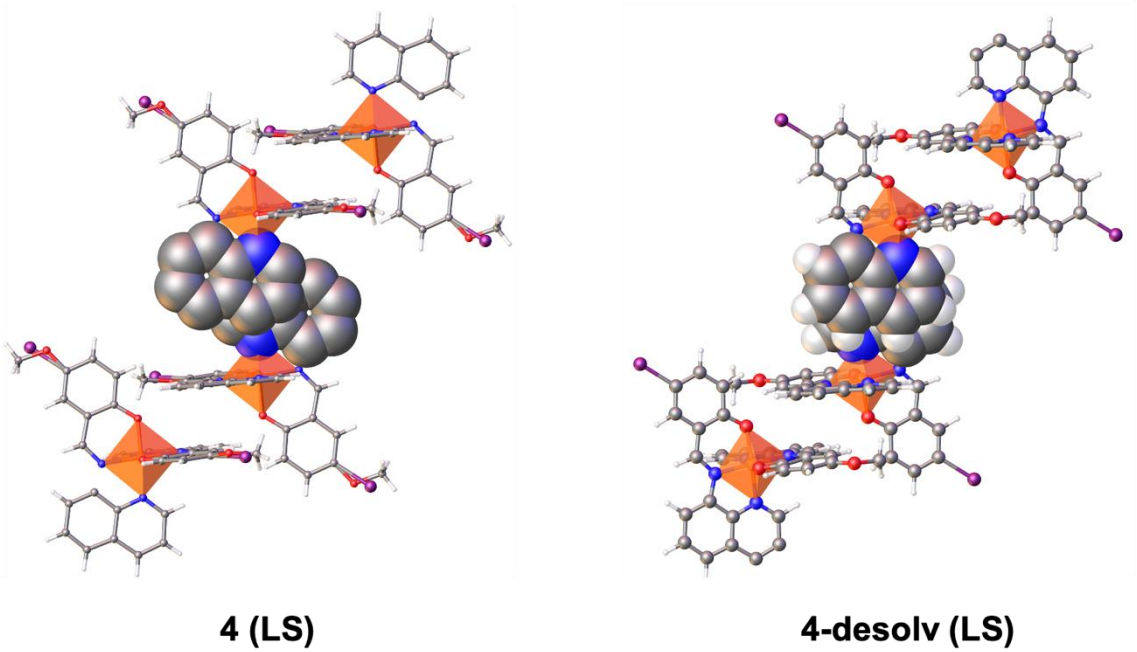

Figure S30: Comparison of π-π interactions in 4 (LS state) (left) and 4-desolv (LS state) (right).

Table S14: Distances between the chains (d_{chain}) and the planes (d_{plane}) at different spin state (LS = low spin, HS = high spin) for **4** (experimental), **4** (simulated) and **4-desolv** (simulated).

	LS		HS	
	d_{chain}	d_{plane}	d_{chain}	d_{plane}
4 (experimental)	12.277	12.765	11.933	13.144
4 (simulated)	12.299	12.795	12.149	13.146
4-desolv (simulated)	11.591	12.670	12.012	13.079

Table S15: Cell parameter *a*-axis, *b*-axis and *c*-axis (Å) at different spin state for **4** (experimental), **4** (simulated) and **4-desolv** (simulated).

	LS			HS		
	a axis	b axis	c axis	a axis	b axis	c axis
4 (experimental)	12.27	12.40	12.76	11.93	12.68	13.14
4 (simulated)	12.29	12.48*	12.79	12.14	12.37*	13.14
4-desolv (simulated)	11.59	12.51*	12.67	12.01	12.31*	13.07

*Simulated structures correspond to supercell (1x2x1), and therefore the values have been divided by 2.

Table S16: Angle between the ligands for **4** (experimental), **4** (simulated) and **4-desolv** (simulated).

	LS angle	HS angle
4 (experimental)	86.6°	84.9°
4 (simulated)	84.0°	83.4°
4-desolv (simulated)	89.4°	78.5°

References

1 S. Hayami, Z. Z. Gu, H. Yoshiki, A. Fujishima and O. Sato, Iron(III) spin-crossover compounds with a wide apparent thermal hysteresis around room temperature, *J. Am. Chem. Soc.*, 2001, **123**, 11644–11650.

2 K. Takahashi, T. Sato, H. Mori, H. Tajima, Y. Einaga and O. Sato, Cooperative spin transition and thermally quenched high-spin state in new polymorph of $[Fe(qsal)_2]I_3$, *Hyperfine Interact.*, 2012, **206**, 1–5.

3 M. Nakaya, K. Shimayama, K. Takami, K. Hirata, A. S. Alao, M. Nakamura, L. F. Lindoy and S. Hayami, Spin-crossover and LIESST Effect for Iron(III) Complex Based on π–π Stacking by Coordination Programming, *Chem. Lett.*, 2014, **43**, 1058–1060.

4 W. Phonsri, P. Harding, L. Liu, S. G. Telfer, K. S. Murray, B. Moubaraki, T. M. Ross, G. N. L. Jameson and D. J. Harding, Solvent modified spin crossover in an iron(III) complex: phase changes and an exceptionally wide hysteresis, *Chem. Sci.*, 2017, **8**, 3949–3959.

5 Z.-Y. Li, Y.-Y. Wu, Y. Li, J.-H. Wang, A. Sulaiman, M. K. Javed, Y.-C. Zhang, W. Li and X.-H. Bu, Slow Phase Transition-Induced Scan Rate Dependence of Spin Crossover in a Two-Dimensional Supramolecular Fe(III) Complex, *CCS Chem.*, 2022, 1–11.

6 S. Kang, Y. Shiota, A. Kariyazaki, S. Kanegawa, K. Yoshizawa and O. Sato, Frontispiece: Heterometallic Fe III /K Coordination Polymer with a Wide Thermal Hysteretic Spin Transition at Room Temperature, *Chem. - A Eur. J.*, 2016, **22**, 532.

7 N. Phukkaphan, D. L. Cruickshank, K. S. Murray, W. Phonsri, P. Harding and D. J. Harding, Hysteretic spin crossover driven by anion conformational change, *Chem. Commun.*, 2017, **53**, 9801–9804.

8 T. Boonprab, S. J. Lee, S. G. Telfer, K. S. Murray, W. Phonsri, G. Chastanet, E. Collet, E. Trzop, G. N. L. Jameson, P. Harding and D. J. Harding, The First Observation of Hidden Hysteresis in an Iron(III) Spin-Crossover Complex, *Angew. Chem. Int. Ed.*, 2019, **58**, 11811–11815.

9 W. Phonsri, Walailak University, 2014.

10 W. Phonsri, D. J. Harding, P. Harding, K. S. Murray, B. Moubaraki, I. A. Gass, J. D. Cashion, G. N. L. Jameson and H. Adams, Stepped spin crossover in Fe(III) halogen substituted quinolylsalicylaldimine complexes, *Dalton Trans.*, 2014, **43**, 17509–17518.

11 D. Sertphon, D. J. Harding, P. Harding, K. S. Murray, B. Moubaraki, J. D. Cashion and H. Adams, Anionic Tuning of Spin Crossover in Fe III –Quinolylsalicylaldiminate Complexes, *Eur. J. Inorg. Chem.*, 2013, **2013**, 788–795.

12 D. J. Harding, W. Phonsri, P. Harding, I. A. Gass, K. S. Murray, B. Moubaraki, J. D. Cashion, L. Liu and S. G. Telfer, Abrupt spin crossover in an iron(III) quinolylsalicylaldimine complex: structural insights and solvent effects, *Chem. Commun.*, 2013, **49**, 6340.